NASA Contractor Report 179576

Size and Shape of Solid Fuel Diffusion Flames in Very Low Speed Flows

(NASA-CR-179576) SIZE AND SHAPE OF SOLID FUEL DIFFUSION FLAMES IN VERY LOW SPEED FLOWS M.S. Thesis. Final Report (Case Western Reserve Univ.) 122 p CSCL 21D

N87-21129

Unclas G3/28 43595

David W. Foutch

Case Western Reserve University
Cleveland, Ohio

February 1987

Prepared for the
Lewis Research Center
Under Grant NGT-36-027805

NASA
National Aeronautics and Space Administration

SUMMARY

The effect of very low speed forced flows on the size and shape of a solid fuel diffusion flame are investigated experimentally. Flows due to natural convection are eliminated by performing the experiment in low gravity. The range of velocities tested is 1.5 cm/s to 6.3 cm/s and the mole fraction of oxygen in the O_2/N_2 atmosphere ranges from .15 to .19. The flames did not reach steady state in the 5.2 seconds to which the experiment was limited. Despite limited data, trends in the transient flame temperature and, by means of extrapolation, the steady state flame size are deduced. As the flow velocity is reduced, the flames move farther from the fuel surface, and the transient flame temperature is lowered. As the oxygen concentration is lowered the flames move closer to the fuel sample and the transient flame temperature is lowered. With stand off distances up to 8.5 $\pm$.7 mm and thicknesses around 1 or 2 millimeters, these flames are much weaker than flames observed at normal gravity. Based on the performance of the equipment and several qualitative observations, suggestions for future work are made.

ACKNOWLEDGEMENTS

While many people have been of great help to me in this work, I am most deeply grateful to Ray Sotos and Steve Kovach for their help in the design and construction of the apparatus, to Dave Clinton and Onetha Mikell for their assistance with the preparation of this manuscript, and to Sandy Olson, Kurt Sacksteder, Howard Ross, and the rest of the Space Experiments Office for many lively and useful discussions. It has been a pleasure to work with my advisor, Dr. James S. T'ien. For his outstanding advice and encouragement, much of the credit for this work must go to him. Finally, I am very thankful for the support of a NASA Graduate Researcher's Fellowship.

TABLE OF CONTENTS

			Page
SUMMARY			i
ACKNOWLEDGEMENTS			ii
LIST OF FIGURES			iv
CHAPTER I	--	INTRODUCTION	1
CHAPTER II	--	APPARATUS	4
CHAPTER III	--	RESULTS	16
CHAPTER IV	--	CONCLUSION	41
REFERENCES			46
TABLES			48
FIGURES			51
APPENDIX A	--	ERROR ANALYSIS	67
APPENDIX B	--	DESCRIPTIONS OF EACH TEST	75
APPENDIX C	--	TRANSIENT DIMENSION DATA	86

LIST OF FIGURES

Figure		Page
1	Schematic Diagram of the Zero Gravity Facility	51
2	Cross-Sectional Schematic of Combustion Chamber	52
3	Combustion Chamber and Drop Package	53
4	Position of Fuel Sample, Sample Holder, and Igniter Wires	54
5	Drive Mechanism and Ignition Mechanism	55-56
6	Section View of Slider Assemble	57
7	Flame Appearance at End of Drop	58-59
8	Flame Dimensions	60
9	Variation of Flame Appearance with V and X_{02}	61
10	Variation of Stand Off Distance with V and X_{02}	62
11	Variation of Flame Width with V and X_{02}	63
12	Variation of Flame Shape Ratio with V and X_{02}	64
13	Variation of Flame Thickness with V and X_{02}	65
14	Variation of Flame Length with V and X_{02}	66
A.1	Distortion of Length Between LED and Front of Sample	74
C.1-C.28	Flame Dimensions vs Time for Data Points 3, 4, 5, 8, 11, and 12	87-114

CHAPTER I

INTRODUCTION

That hot air rises is a widely known fact. The flow induced by this rise, termed natural convection, affects any flame influenced by the Earth's gravitational field. Since the induced flow is a product of the flame, it is difficult to perform a combustion experiment in which the flow velocity is an independent variable. One approach is to investigate velocities much higher than the induced velocities, so that the effect of natural convection is relatively small. If one wishes to investigate the effect of a low speed forced flow on a flame, the natural convection must be eliminated. This can be done only by performing the experiment in a low gravity environment.

Kimzey, et al, [1] performed many experiments in an airplane flying a parabolic trajectory to achieve low gravity. These experiments used a variety of fuels and attempted to rate their flammability in zero gravity. Other combustion experiments have been performed in drop towers. Andracchio and Cochran [2] measured flame spread rates over very thin solids in low gravity. Kumagai and Isoda [3] performed droplet burning experiments that were undisturbed by natural

convection.

Okajima and Kumagai [4] described flames around moving droplets in low gravity, with velocities less than 2 cm/s. As far as the author knows, this is the only combustion experiment performed with such low velocities. No experiments have been performed for solid fuels at these low velocities. This experiment, then, will investigate the nature of diffusion flames above a solid fuel in very low speed forced flows.

An absence of data in this flow regime is not the only motivation behind this work. Recently T'ien [5] performed a calculation for a stagnation point flame, with PMMA as the fuel. When surface radiation was included in the model, a low speed extinction limit was found. Foutch and T'ien [6] extended the calculation to the mixed convection case and found the same result. Chen [7,8] performed a calculation for a flame stabilized at the leading edge of a thin fuel plate. Including radiation in this model also resulted in a low speed extinction limit. So these calculations predict that, at a given oxygen concentration, there are two limiting speeds: the high speed blow off limit, analogous to blowing out a match, and a low speed radiative limit. This experiment will attempt to verify the existence of the low speed limit.

To eliminate natural convection the experiment is performed in the larger of NASA Lewis Research Center's drop towers, the Zero Gravity Facility. The low flow velocities are obtained by moving the fuel sample through the quiescent atmosphere inside a combustion chamber. The only data taken are high speed motion pictures of the flame.

In the remainder of this report, the apparatus and the decisions behind the design of the equipment are discussed. Then the results are presented, including the performance of the equipment, qualitative descriptions of flame shape and color, and quantitative flame dimensions. The flame dimensions are compared to Chen's calculations for this geometry [7,8,9]. At the end the results are summed up and recommendations are made for further work.

CHAPTER II

APPARATUS

II.1 The Zero-Gravity Facility

Since the decision to utilize the Zero Gravity Facility greatly influenced the design of the experiment, the facility and its operation will be described first. This facility is essentially a giant, steel-walled vacuum chamber. Figure 1 is a cut away view of the Zero Gravity Facility. It is 6.1 meters in diameter and extends 145 meters beneath the ground. To prepare for a drop, the drop package, which consists of the experimental apparatus, a frame to support it, and a protective cover, is suspended at the top of the chamber by a single notched bolt. The chamber is evacuated to 1.3 Pascals (1.3×10^{-5} atm) to minimize the air drag on the drop package. When the signal to start the drop is given, the notched bolt is sheared and the drop package falls freely. At the bottom the package is decelerated without damaging the equipment as it plunges into a large container filled with polystyrene beads.

The shearing of the bolt imparts no significant rotation to the drop package and there is no

significant air drag, so the resulting gravity level experienced by the drop package is very low -- less than 10^{-5} g's (9.8×10^{-5} m/sec2). The duration of free fall is 5.2 seconds, limited of course by the distance the package can fall, 132 meters. The deceleration at the bottom averages 35 g's (340 m/sec2) for 120 milliseconds. The nature of the Zero Gravity Facility, then, requires that the experiment be automated, that the apparatus can survive the deceleration at impact, and that the experiment last no more than 5.2 seconds. This 5.2 second limitation is the most severe and it played a large part in the design of the experiment.

II.2 The Combustion Chamber and the Drop Package

The combustion chamber has been used for several different experiments. It is adequate, but not ideal for this experiment. Building a new chamber, though, would have been quite expensive and would have taken many months. The chamber that was used is shown in Figure 2. It is made of .48 centimeter (3/16 inch) thick stainless steel, with an internal volume of 113 liters. The chamber was designed to hold a vacuum so that it could easily be filled with any desired atmosphere, for this experiment a mixture of oxygen and nitrogen. The inside diameter is 39.6 centimeters and

the height from the bottom of the chamber to the lower flange is 25.4 centimeters. When the chamber is opened the top half slides to one side, clearing the bottom half by about one centimeter. This means that all the experimental apparatus that is to go inside the chamber must fit in the bottom section.

The chamber is mounted on a supporting frame, as seen in Figure 3. Batteries to power the ignition system, the high speed camera, and the other electronics are mounted beside the chamber. There are several time delay relays to control the experiment during the drop. The combustion chamber has two viewing ports, one on the side of the chamber, 12.7 centimeters from the bottom, and another at the top. There is a camera mount on the frame for each port. A metal cover protects the apparatus and ensures the proper flow of styrofoam beads around the drop package so that the beads will decelerate it safely at the end of the drop.

II.3 The Camera and the Film

A Teledyne high speed motion picture camera mounted at the top view port is used to record the results of the experiment. The camera can run at up to 400 frames per second, but in order to provide an

exposure long enough to see the flame the camera is run at 60 frames/sec. The camera is 65 cm from the fuel sample. The main advantage of using the top view port rather than the side view port is that the entire travel of the sample can be seen with almost no distortion from the lens. The biggest disadvantage is that the resolution is not very good because the camera is so far from the sample. The film is 16 mm Kodak Ektachrome high speed video news film, SO251. This film is used for experiments in the Zero Gravity Facility because it does not degrade when exposed to a vacuum. The film is force processed 2 f-stops to enhance the image of the dim blue flame.

II.4 Fuel

The choice of fuel was affected by the time limitation imposed by the drop tower and by the nature of the experiment itself. If this experiment is to investigate the effect of radiation from the fuel surface then a fuel must be chosen that has a high surface temperature when burned. Also the fuel must be thin in order to minimize the ignition time. The fuel used for the experiment is nonadecane held in a Fiberfrax wick.

Nonadecane ($C_{19}H_{40}$) is a straight chain hydrocarbon. At room temperature it is a waxy solid;

it melts at 306 K and boils at 603 K. Its other properties are listed in Table 1. When most liquid fuels burn the surface temperature is very near to the boiling temperature [10]. So the surface burning temperature of nonadecane should be near 603 K. Some typical surface temperatures for burning solids in oxygen/nitrogen mixtures are: 700 K for PMMA in 16% O_2 [11], 730 K for polystyrene in 17% O_2 [11], and 673 K for paper in air [12,13]. Comparing the fourth power of the boiling temperature of nonadecane to the fourth power of the surface temperatures of these burning solids shows that the radiative heat loss from the burning nonadecane is about 45% - 65% of that from a typical solid. The results of Olson and T'ien [14] suggest that even reducing the surface radiation by 60% produces a significant effect on the extinction limit. Since the emissivity of the fuel sample is expected to be about the same as that of paper or PMMA, the surface temperature of the burning nonadecane is high enough for the effects of the surface radiation to be observed.

Fiberfrax is used in industry as an insulator for furnaces and for other high temperature applications. It is made of SiO_2 and Al_2O_3 and can withstand temperatures up to 1260°C without degrading. Its

properties are listed in Table 2. It is a spongy, absorbent material, manufactured in several thicknesses. The thinnest Fiberfrax is used for this experiment, .08 cm (1/32 in).

The fuel samples are made by dipping a small piece of Fiberfrax into melted nonadecane, allowing the nonadecane to solidify, and then cutting the sample to size, 3.75 cm X .63 cm (1.5 in X .25 in). This procedure is done under carefully controlled conditions. First many slightly over-sized Fiberfrax samples are baked at 130° C under a vacuum of 1 Pascal (10^{-5} atm) for several hours to remove any moisture and contaminants. These samples are stored inside a plastic bag in a dry box, which keeps the relative humidity of the air less than 5%. The samples are prepared inside the dry box. The pieces of Fiberfrax are dipped into the melted nonadecane and, in order to insure that the fuel is distributed evenly through the wick, the sample is turned slowly, like a pig on a spit, while the nonadecane solidifies. Then the samples are cut to size: 1.5 in by .25 in. Finally the samples are weighed to determine the area density of fuel. The total area density of every sample falls in the range 72 - 86 mg/cm2, measured to an accuracy of $\pm$ 4 mg/cm2. Accounting for the area density of the

Fiberfrax, 12.4 $\pm$ .1 mg/cm2, the fuel area density is 60 - 74 $\pm$ 4 mg/cm2. The fuel samples are not stored in the dry box after they are made. It is assumed that the waxy nonadecane will not absorb any moisture from the air.

The resulting fuel sample is basically a candle -- an absorbent wick impregnated with a waxy solid. It also burns like a candle. The nonadecane melts when heated by the igniter and vaporizes from the fuel surface. A diffusion flame is then established above the fuel surface. Liquid nonadecane is wicked to the surface to replace the vaporized fuel. This system is also a good simulation of a solid burning. Instead of pyrolyzing, the nonadecane vaporizes. Instead of the fuel surface charring and receding, the liquid nonadecane is wicked to the surface.

This difference between the fuel/wick system and a typical solid makes the fuel/wick system the better choice for this experiment. If the fuel surface were to recede or char during the course of the experiment the flow around the sample would be changed in an unpredictable way. For a thin fuel a receding fuel surface implies a spreading flame. Spreading velocities of several centimeters per second are not uncommon [15] and the spreading velocity depends on the

environment the flame is in. For this experiment, the velocity of the oxidizer relative to the flame is to be an independent variable and since the velocities to be investigated here are also a few centimeters per second, a non-spreading flame is required. The fuel/wick system meets this requirement.

Figure 4 shows the fuel sample mounted in the holder and the position of the fuel sample relative to the igniter wires. The holder insures that the flame is quenched at the end of the sample. This makes the flame three dimensional near the edges, but only a small portion of the width of the flame is affected, so the center part of the flame remains two dimensional. The width of the sample exposed to the flame, 2.5 cm (1 in) was chosen from past work [15] and preliminary testing to give a two dimensional flame. The length of the sample in the streamwise direction is kept small, .63 cm (.25 in), to make the sample easier to ignite and, since the whole surface is burning, to insure that the flame is not spreading downstream.

The holder is made of four L-shaped pieces of spring steel. It was designed to be as thin as possible to allow the flame to be seen well and to minimize the flow disturbance from the holder. The holder is wide enough so that the tail of the flame is

not visibly affected.

II.5 Ignition System

The fuel sample is ignited by a pair of hot nichrome wires, 1.0 mm in diameter and approximately 34 cm long. As shown in Figure 4, the wires are bent in such a way to give even heating over the fuel surface while the sample travels between them. There is a gap of about 2 mm between the sample and each wire. To ignite the sample, the power to the wires is turned on at the start of the drop: 32 volts are applied across the wires and 55 amps flow through each wire. It takes about .5 seconds for the wires to get red hot. Preliminary tests in normal gravity indicated that the delay between the time the wires get hot and the time the sample is ignited is about one second, so power to the wires is turned off 1.5 seconds into the drop. To keep the ignition conditions the same for each drop, the speed of the sample as it is being ignited is always 3.7 cm/s.

II.6 Drive Mechanism

In order to obtain a uniform flow of oxidizer, the sample is moved through the quiescent atmosphere. It was felt that it would be very difficult to obtain a uniform flow of air past a stationary sample at such

low velocities. The drive system used to move the sample is shown in Figure 5. It consists of two guide rods, a lead screw, and a sliding block. The sample holder is mounted to this block. Linear bearings allow the sliding block to move easily on the guide rods. The sliding block floats on a nut threaded on the lead screw, as shown in Figure 6. As the lead screw turns, the sliding block is driven along the guide rods. Since the sliding block floats, no forces are transmitted laterally and the motion is not affected by any eccentricities in the lead screw.

The lead screw is driven by a DC electric motor, through a 16:1 gearbox and an additional set of gears. The additional gears are used to keep the length of the drive system as short as possible, since it has to fit in the bottom section of the combustion chamber. Choosing the appropriate gearing, the top speed of the drive system is 50 cm/s. With the limited distance and time, though, the highest speed that can be observed for the entire drop is 6.3 cm/s. Tests at higher speeds would have to be less than 5.2 seconds long. The electronics that control the motor allow for two speeds to be selected for each test. The time delay relays control when the motor is turned on and when the speed change, if any, occurs.

II.7 Experiment Procedure

Normally one drop per day is done at the Zero Gravity Facility. This drop is done in the morning. The afternoon before a drop the drive mechanism is calibrated to the correct speed and the time for the speed change is set. The next morning the apparatus is fastened to the floor of the combustion chamber and the chamber is sealed. The chamber is then evacuated and filled with the proper mixture of oxygen and nitrogen. All tests were done at a pressure of one atmosphere, 14.7 psia. The drop package is mounted in position at the top of the drop tower and the air in the tower is pumped out. When the signal to start the drop is given, the bolt is sheared by remote control and the package starts to fall.

The sequence of events during the drop is controlled by a set of time delay relays. The time set for the speed of the motor to change is denoted as T_0. For most tests, T_0 is 1.5 seconds. For tests at very low velocities, T_0 is 3.0 seconds to insure that the sample will be far enough from the igniter at the end of the drop. The sequence of events is:

t=-2.0 sec : Internal lights turned on; camera turned on.

t=0.0 sec : Drop starts; Internal lights turned off; Power to igniter wires turned on.

t=0.5 sec : Motor starts to drive sample.

t=1.5 sec : Power to igniter turned off.

$t=T_0$: Motor speed changed.

t=5.2 sec : Drop ends. Air in chamber vented to the surrounding vacuum.

The drop package is then recovered and the burned sample is saved.

II.8 Data Analysis

A motion analyzer is used to extract the data from the film. The three essential components of the motion analyzer are the screen, the cursor, and the coordinate display. The film is back projected onto the screen and stopped at the desired frame. When the cursor is placed on the screen the frame number and the x and y coordinates of the cursor, relative to an origin fixed to the screen, appear on the display. Pushing the cursor button transmits this information to a personal computer. Several BASIC programs are used to collect the data, translate it into physical dimensions, and plot the results.

CHAPTER III

RESULTS

II.1 Evaluation of Equipment

Since a large part of the work behind this project involved the design and construction of the equipment, it is appropriate to spend some time discussing the success of the design. Also, the quality of the data depends largely on the equipment, so the quality of the data will also be discussed here.

The least reliable part of the apparatus is the ignition system. The igniter wires draw a huge amount of current: 105 amps at 32 volts, or over 3200 watts. When everything was working right this presented no problem. But such a demand on the electrical system magnified every weakness in the system. Several times a single cell in the bank of batteries went bad, reducing the power to the wires enough to prevent the sample from igniting. If the load on the system had been smaller, the failure of one cell would not have had as severe an effect. This problem was aggravated by the need to wait three days for film processing to see the results of a test. During these three days another test would occur. When a cell went bad, two tests were affected instead of one. And the number of

tests is severely limited by the demand for using the Zero Gravity facility and by the cost of each test.

Even with enough power, though, proper ignition is difficult to achieve. In some tests only a portion of the sample ignited and the flame spread across the sample during the test. This spread was very slow and the flame front often remained flat, indicating that the flame was two dimensional. Some reliable data was obtained from these tests. Also, it is possible to have too much power. The problem with the cells was repaired and the electrical connections between the batteries and the igniter wires were strengthened. The wires got much brighter for these tests and the ignition was too powerful. The initial ball of flame generated was so large that when the sample emerged from between the wires, the heat feedback rate from the initial ball of flame was too low to sustain combustion.

Despite these competing problems, the first several drops ignited well and provided good data. On the last few drops the ignition was too strong and on the drops in between the ignition was often too weak. A further description of the results of each drop can be found in Appendix B.

The DC electric motor presented a minor problem.

It behaved differently when cold than when warmed up. It warmed up during calibrating, but it was dropped while cold, so the sample did not always travel at the desired speed. Only two tests were affected to a large degree by this problem. Although they ran at the wrong speed, the speed was constant and the tests provided useful results, though not as useful as they could have been. This problem can be fixed in future work by using a stepper motor to have more exact control over the position of the sample.

The ignition system can be improved by using a shorter igniter wire that moves with the sample during the ignition phase of the drop. The smaller wire would draw less power and would not be as susceptible to weaknesses in the electrical system. Further work needs to be done to assure that the sample ignites across its entire width.

Despite these equipment problems some good data were obtained. The sample proved to be the correct width for a two dimensional flame to form. The sample moved smoothly at a constant speed and the flames were symmetric about the sample. Useful qualitative information could be extracted from some of the less-than-perfect tests.

III.2 General Description of Results

Before starting a detailed analysis of the results, the general nature of the flames will be discussed. None of the flames reached steady state. In all but one test the flame grew throughout the drop, moving farther from the sample. So to draw any conclusions about steady state flames, some assumptions will have to be made. These will be introduced later. Also, when comparing the results of different drops, the rate of change of the particular result in question must be accounted for. Flame extinction was not observed, so no direct evidence of a low speed extinction limit was found. The trends in the results wil be examined for any indirect evidence of this limit.

Figure 7 shows the appearance of the flame at the end of the drop for six different tests. There are two views of each flame. The pictures in the left column are the plan views of the flames as viewed in the mirror (see Figure 5). The pictures in the right column are the edge views of the flames and the samples, seen directly by the camera. The relative position of the sample to the flame is indicated in each photograph. The scale in all the photographs is the same, about 1.25 times larger than actual size.

The edge view is brighter because there is much more depth to the flame in this view. In the plan view one is looking through the thinnest part of the flame, so the flame is much dimmer. Figure 8 is a schematic representation of the edge view of the flame and its relation to the fuel sample.

In all cases the flame is brightest at the front of the flame, that part of the flame ahead of the sample as it moves. In these pictures the sample is always moving from left to right. The flame becomes dimmer and dimmer downstream of the front of the flame, until at some point the flame is no longer visible. This point marks the end of the visible flame. This region downstream of the sample will be called the tail of the flame. The part of the flame farthest upstream will be called the leading edge of the flame.

These flames are very different from those observed during the testing of the equipment at normal gravity. The normal gravity flame was a thin blue sheet very close to the fuel surface, with a long yellow tail. These flames are very thick, 1 or 2 millimeters, and are very far from the fuel surface, with stand off distances up to 8 millimeters. Only one of the low gravity flames had a yellow tail and this tail was much shorter than that of a normal gravity

flame. So the flames found in this experiment are very weak, low powered flames, much different from most flames that are observed in normal gravity.

III.3 Test Conditions and Repeatability

The conditions of the twelve tests that provided data are shown in Table 3. The accuracies of the test conditions are discussed in Appendix A. Two-dimensional flames are observed in six of the tests. In the other six, marked by an asterisk, the sample was not ignited properly and the resulting flames are not two-dimensional. While these tests cannot be used for quantitative comparisons with the two-dimensional flame results, it is felt that some useful qualitative information can be obtained from them.

Only data points 5 and 10 were repeated. For the first test at point 5 the camera was poorly focused, so these two tests can only be compared qualitatively. The shape of the flame and the transient from a blue to a yellow flame are very similar for the two tests. There is no discernible difference between the two tests, though there may be some differences that are hidden because the first test was out of focus. The flames of the two tests at point 10, neither of which is two-dimensional, are somewhat different. One flame is dim blue, while the other is bright blue with some

yellow at the leading edge of the flame. The flame dimension data do not agree either. These inconsistencies between the two tests are assumed to be attributable to the differences in the ignition. Because the flames at data point 10 are not two-dimensional, it is difficult to judge the repeatability of the flames that are. Instead of comparing results of repeated data points, the data will be examined for consistency between data points to judge the repeatability of the measurements.

III.4 Method of Presentation

Many of the results of the drops are presented as in Figure 9. The position on the graph gives the test conditions, the velocity of the sample, V, and the mole fraction of oxygen in the atmosphere, X_{02}. The caption beside the point gives the result of the test, for this case the appearance of the flame. This "map" of the results is used because, especially with the flame dimension data, there are not enough data points to justify drawing a curve through them. Only the general trends can be deduced from the data and it is easier to see trends with these maps.

III.5 Flame Shape and Color

While qualitative, the shape and color of the

flame are very useful information. The color of the flame will be discussed first. Two colors are seen in these flames, blue and yellow. The blue part of a flame is usually a thin sheet. The flame is blue because one of the many reactions occurring in the flame releases a photon as one of the products. The temperature dependence of the rate that this particular reaction occurs is different from that of the rates of the other reactions occurring in the flame. Below a certain temperature, the photon-producing reaction is proceeding too slowly to produce enough photons for the camera to detect, but other reactions are still occurring. So the blue part of a flame marks the visible reaction zone, while the low temperature part of the reaction zone cannot be detected by the camera. Since the film was force processed the yellow regions are usually over-exposed. So the yellow zones are very bright, often nearly white, and no structure is visible inside these zones. The yellow part of the flame is caused by glowing soot particles. The formation of soot is governed by a combination of two factors, the flame temperature and the gas residence time in the reaction zone. All else being equal, for the flames in this experiment, increasing the flame temperature will increase the amount of soot formed. Similarly,

increasing the residence time -- either by decreasing the velocity of the gas or increasing the thickness of the flame -- will lead to more soot, if the temperature does not change. This soot formation model will be used to explain the flame color results.

The yellow regions observed in the flames do not reach a steady state, but if soot forms during a test, it always forms in the same manner. First a blue flame is established around the sample. The soot starts to form at the leading edge of the flame and then the soot zone spreads downstream. Next another region of soot forms in the tail, downstream of the sample. Now there are two regions of soot, with a blue reaction zone between them. These two regions merge very quickly and the soot spreads throughout the tail region. Referring to Figure 9, only two tests, data points 1 and 5 show some sign of soot in the tail. Of these, only point 5 shows the soot spread through the tail. In four other test -- 3, 4, 10a, and 12 -- soot started to form in the leading edge, but did not spread any farther. The flames in the remaining tests were all blue.

Can any trends be deduced from this data? Comparing points 2, 3, 4, and 5, shows the trend that less soot is formed at lower velocities. Comparing 10a and 11, however, shows the opposite trend. Also,

lowering the oxygen concentration should reduce the flame temperature and, therefore, should reduce the amount of soot formed. This trend is shown by points 5, 6, and 11. However, more soot formed at point 12 than at either point 3 or 4, reversing the expected trend. These anomalies, which are assumed to be attributable to variations in the ignition of the sample, make it impossible to draw conclusions about soot formation by comparing just two points. Nevertheless a conclusion can be drawn by observing the general trends among all data points. It is clear that more soot formed at points 1 and 5 than at any other point. These points are at the upper right portion of the "map," at the highest velocities and oxygen concentrations. All of the tests at lower velocities or oxygen concentrations showed less soot. So lowering velocity and oxygen concentration reduce the transient soot formation.

This trend in transient soot formation can be linked to a trend in transient flame temperature. Since the gas residence time is being increased with lower velocity one would expect more soot to be formed at lower velocities. Instead less soot forms, indicating that, despite increasing the residence time, lowering the velocity lowers the temperature. A

similar trend is seen for lowering the oxygen concentration, which lowers the flame temperature and thereby reduces the amount of soot formed.

The fact that yellow flames start as blue flames and progress through a series of steps until becoming all yellow raises the obvious question: will the flames that remained blue throughout the test turn yellow, given enough time? It is possible that the reason soot has not formed in the lower velocity flames is that these flames simply have not had time to develop. So the only conclusion that can be drawn from the flame color data is that the flames at lower velocities and oxygen concentrations are cooler during the first five seconds than the flames at the higher velocities and oxygen concentrations.

As discussed above, the brightness of a blue flame is related to the reaction rate in the flame. The brighter the flame is, the faster the reaction is proceeding. The blue part of the flame in most of the tests were all about the same brightness. Only points 2, 7, 8, and 9 were noticeably dimmer. These tests were done at the lowest velocities. Again, no firm conclusion can be drawn, but this is an indication that the flames at lower velocities have lower reaction rates.

The flame shapes provide another clue. These shapes refer only to the blue part of the flames, so nothing can be said about the shape of the flame at point 5 after soot obscured the tail. Two types of shapes are observed, closed flames and open flames. For closed flames a blue reaction zone surrounds the fuel sample. For open flames, as seen in Figure 7, there is a break in the blue reaction zone in the tail of the flame. The tails of the open flames always curve back toward the fuel surface. Determining flame shape is not a simple task. The flame is brightest at the leading edge and gets dimmer and dimmer in the downstream direction. It is very difficult to tell just where the flame tail ends. It is often very difficult to tell whether the flame is open or closed. Also, the flame brightness in the tail varies during some tests. Sometimes a closed flame forms, then changes to an open flame, and then changes back to a closed flame. The flame shape is not a precise measurement so only general trends can be discussed.

The flames at points 1 and 5 are closed for as long as they can be seen. The flame at point 4 starts closed, but has a very dim tail. The tail dims through the test and at the end of the test the flame is open, with the tails curving back toward the fuel surface. A

flame which changes from open to closed, and back again, is observed at point 11. It is open during most of the test, closing once or twice for very brief periods. When it is open, the tails always curve back toward the fuel surface. The flames at points 3, 8, 10, and 12 were open and the tails always curved back. The flames at points 2, 7, and 9 did not provide reliable shape data.

The effect of velocity on the flame shape can be seen in Figure 7, which shows the flames just before the drop ended. As the velocity is lowered the flame becomes "more open." The tail does not curve back as much and the ends of the tail are farther apart. Also, the point that the tail starts to curve back toward the fuel surface moves downstream with lowered velocity. No trend can be seen for varying the oxygen concentration with this data. The lengths of all of these flames are about equal. To sum up the flame shape results, closed flames are observed only at the highest speeds and oxygen concentrations tested. As the speed and the oxygen concentration are lowered the flames become more and more open.

There are two ways to explain the differences between an open and a closed flame. The first involves the invisible reaction zone discussed above. If there

is a temperature below which the reaction that produces the blue photons will not proceed, then it is possible that there is still a reaction occurring in the tail of the open flame, but at a temperature too low to produce these photons. The second explanation is that there is no reaction at all occurring in the open tail of the flame, due either to a lack of oxygen, a lack of fuel, or too low a temperature. There is no way to distinguish between these two cases with just pictures of the flames. In either case, the reaction rate in the tail of open flames is lower than that of closed flames, so open flames are, in this sense, weaker than closed flames.

III.6 Flame Dimensions

Only six tests gave results that were reliable enough to take quantitative flame dimensions from the films. The dimensions measured are shown in Figure 8. All dimensions, except for flame thickness, are measured from the outside edge of the visible flame. This edge is used, rather than the middle of the blue reaction zone, because some of the flames are yellow. The yellow, caused by glowing soot particles, obscures the blue reaction zone. Because soot forms on the fuel rich side of a diffusion flame, the outer

edge of the yellow zone can be assumed also to be the outer edge of the blue reaction zone, and it is the reaction zone which defines the flame. This is not necessarily true for the tail of the flame, however. The glowing soot can be convected downstream beyond the reaction zone, so that the reaction zone is completely obscured.

Referring to Figure 8, the width of the flame, W, is defined at the leading edge of the sample. It is the distance in the cross-stream direction between the outer edges of the flame. The stand off distance, S, is measured from the leading edge of the sample to the leading edge of the flame, the point of the flame farthest upstream. A flame shape ratio, A, is defined as the ratio between the width and the stand off distance. The flame thickness, T, is measured from the leading edge of the flame to the inside edge of the reaction zone downstream of the leading edge. The length of the flame, L, is measured from the front of the flame to the end of the flame. For cases where the tail of the flame is open, the length is the average of the lengths of the two tails. The accuracy of these measurements is discussed in Appendix A.

Two accuracies are used for the stand off distance and the flame shape ratio. There are two sources of

error in the stand off distance measurement, one of which depends on the position of the sample. If the sample is in the same position for different tests, then this error is the same in both cases. These two tests can be compared more accurately than two tests when the samples are in different positions. So when comparing between tests at the same velocity, or when comparing between two times that are close together on the same test, the "second accuracy" shown in Figures 10 and 12 can be used. When comparing flames from tests at different velocities, or at widely different times for the same test, the "first accuracy" must be used. Also, when reporting the absolute magnitude of the stand off distance, the first accuracy must be used. Since the stand off distance is used to calculate the flame shape ratio, similar reasoning applies to it.

The flame dimensions are presented with the value of the dimension at the end of the drop and the rate that this value is changing at the end of the drop, calculated from a least squares curve fit of the last half second of data. The rate of change is often used to extrapolate the trend between two data points to the trend that would result if both the flames had reached steady state. For example, if both the stand off

distance and the rate at which the stand off distance is increasing are higher for one flame than for another, it is assumed that when both flames reach steady state, the first flame will still have the larger stand off distance. No predictions are made on how big the difference will be.

III.6.a Stand Off Distance

Figure 10 shows the variation of stand off distance, S, with the sample velocity, V, and the oxygen mole fraction in the atmosphere, X_{02}, for the six data points. As explained in Appendix A, when comparing tests at the same velocity, the comparison is accurate to $\pm$ .3 mm. When comparing two tests at different velocities, or when reporting the absolute magnitude of the stand off distance, the accuracy is $\pm$ .7 mm. The variable S denotes the value of the stand off distance at the end of the drop, while $\dot{S}$ denotes the rate at which the stand off distance is either increasing or decreasing at the end of the drop. The variation of stand off distance with velocity can be seen by comparing points 3, 4, and 5, at X_{02}=.18, and by comparing points 8 and 11, at X_{02}=.16. At point 3, V=2.4 cm/s, the stand off distance at the end of the drop is 8.4 mm, increasing at 1 mm/s. At point 4, V=3.6 cm/s, the value is 8.5 mm and is

increasing at .6 mm/s. Since the stand off distance is still changing in each case, it is impossible to tell which will have the larger value, although it seems the final value for point 3 will be larger since it is growing faster at the end of the drop. At point 5, V=6.3 cm/s and the stand off distance at the end of the drop is 5.5 mm, increasing at 1 mm/s. From these three points it can be seen that the stand off distance increases as the velocity decreases, although it may not change very much at lower velocities. This trend is also apparent when comparing points 8 and 11. For point 8, X_{02}=.16 and V=1.4 cm/s, the stand off distance is 6.5 mm at the end of the test, increasing at .5 mm/s. For V=6.2 cm/s the stand off distance is 3.4 mm, increasing at 0.2 mm/s. Clearly the stand off distance is larger for the test with the lower velocity.

Physically this trend makes sense. The stand off distance is determined by a balance between heat conduction and convection. As the velocity is decreased, the convection is weakened and heat can be conducted farther upstream, establishing the flame farther upstream and therefore increasing the stand off distance. Chen's work [7,8] demonstrates this trend theoretically.

The effect of oxygen concentration on the flame stand off distance is most clearly seen by comparing points 5 and 11, both at V=6.2 cm/s. The stand off distance for the test at the higher oxygen concentration was larger and increasing faster at the end of the drop than that for the test at the lower oxygen concentration. For point 5, with X_{02}=.18, the stand off distance is 5.5 mm. For point 11, with X_{02}=.16, it is 3.4 mm. So, for these two points, the stand off distance increases with oxygen concentration. This trend is also shown by comparing points 3 and 4 with point 12. For point 12 V=2.9 cm/s. While there was no test at this velocity for X_{02}=.18, it can be assumed the result would lie between those for points 3 and 4. The stand off distances at both points 3 and 4 are larger than that at point 12, as are the rates of increase. The trend that stand off distance increases with increasing X is confirmed by these three points.

This trend occurs because lcwering the oxygen content lowers the flame temperature. Less heat is transferred to the fuel surface and less fuel is vaporized, so the blowing velocity at the wall due to the expansion of liquid fuel to gaseous fuel is lowered. The flame is then forced closer to the surface by the forced flow velocity. Chen's

calculation shows a similar trend [7,8].

III.6.b Width

Figure 11 shows the variation of the flame width with velocity and oxygen concentration. For points 3, 4, and 5, all taken at the X_{02}=.18 the flame width increases as the velocity decreases. The widths are still changing, but the widest flame, point 3, is increasing the fastest, and the other widths are increasing at about the same rate, so it is assumed that the steady state flame widths will follow the same trend as these transient widths. A similar trend is seen by comparing points 8 and 11, taken at X_{02}=.16. At the end of the test, the width is nearly steady in both cases. The final value for point 11, at V=6.2 cm/s, is 1.04 cm, compared to the final value of 1.75 cm for point 8, at V=1.4 cm/s. So the trend of increasing width with decreasing velocity is confirmed by these two points.

The physics behind this trend is the same as that for the stand off distance. The width is determined by the distance the heat and the fuel can diffuse in the cross-stream direction while being convected downstream. This distance increases as the velocity is lowered. Again, Chen's work [7,8] showed this trend.

Figure 11 also shows that the width decreases with decreasing oxygen concentration. The width at point 5 is larger and increasing faster than the width at point 11, so the steady state widths will follow the same trend as the widths at the end of the test: the flame at the higher oxygen concentration is wider. Comparing point 12 to points 3 and 4 also shows this trend. The final value is lower for point 12 than for either point 3 or 4 and the rate of increase is no faster than for either point 3 or 4, so it can be assumed that the steady state width will also be lower. A similar comparison between points 8 and 11 and point 12 is inconclusive because the width at point 12 is increasing faster than that for either point 8 or point 11. Nevertheless, the trend is that the width decreases with oxygen concentration. This follows the trend for the stand off distance. This would be expected because the width and the stand off distance are both determined by the same physical processes.

III.6.c Flame Shape Ratio

The flame shape ratio, A, is defined as the ratio of the flame width to the stand off distance. The variation of A with velocity and oxygen concentration is shown in Figure 12. As explained in Appendix A, when comparing A at points with different velocities, the accuracy on A is .5. When comparing A at points with the same velocity, the comparison is accurate to $\pm$ .2. Due to the greater error, no conclusions can be drawn about the variation of A with velocity at either X_{02}=.18 or X_{02}=.16. Chen [7,8] found that A, within the accuracy of the measurement, remained constant for this velocity range. The only points that can be used to determine the trend with oxygen concentration are points 5 and 11. But A is decreasing at point 11 and is nearly steady at point 5, so the comparison is not very good. There is one weak piece of evidence to show that A decreases with increasing oxygen concentration. Every value of A at points 8, 11, and 12 is higher than any value at either points 3, 4, or 5. Chen's calculation for this geometry showed a that A is nearly constant with varying oxygen concentration, decreasing slightly as the extinction limit is approached. The magnitude of this decrease is less than the error in the measurment here. So the flame shape ratio, A, is

not very sensitive to changes in either velocity or oxygen concentration.

III.6.d Thickness

The results of the flame thickness measurements are shown in Figure 13. No data are given for points 3, 5, and 12 because soot obscured the inside edge of the reaction zone. Measured thickness for these points showed steady growth, while the thicknesses for the other flames remained constant through the test. Because of the large scatter in the data, no meaningful estimate of the rate of change can be made to compare the three tests, so only the final values will be compared. Depending on the position of the sample, these measured thicknesses may be larger than the actual flame thicknesses because of the viewing angle. As the sample moves to the edges of the field of view, the camera is no longer looking straight down on the flame, but rather at a slight angle. This angle would tend to make the flames look thicker than they are. This fact, combined with the large scatter in the thickness data, as seen in Figures C.19 to C.23, make it possible to draw only one conclusion from the thickness data. These flames, with thickness around 1 or 2 millimeters, are much thicker than the flames observed when testing the fuel at normal gravity.

III.6.e Flame Length

The flame length was the most difficult dimension to measure because of the nature of the flames. In all cases the leading edge was the brightest part of the flame. The tails of the flame got dimmer and dimmer with distance downstream. Because of this gradual dimming it was difficult to pinpoint the end of the tail. This problem was aggravated by the need to force process the film to see the blue flames. The force processing enhanced the blue in the film, but it also tended to make some of the grains of the film blue also. Occasionally these blue grains made the flame seem longer than it was. The result of these difficulties is that there is a wide scatter in the length data.

Figure 14 shows the variation with V and X_{02} of the average flame length, L. For data point 5 the soot in the tail obscured the reaction zone, so no length data can be obtained. All of the final values are in the range $1.9 \pm .2$ cm, but the rates of change at the end of the tests are different. There is no pattern to the rates of change at the end of the tests, so no conclusions can be drawn about the dependence of flame length on V and X_{02}.

Examining Figures C.24 - C.28, which show how the

flame length changes with time for each test, provides some explanation for the unusual nature of the flame length results. While points 3 and 12 show no more scatter than could be expected from innaccuracies, points 4, 8, and 11 show rather large fluctuations in length that are more than just measurement error. For points 4 and 11 these fluctuations occur when the flame changes from a closed to an open flame, as discussed in section III.5. While the length of the flame at point 8 fluctuates at the end of the drop, it does not change to a closed flame. So, on top of a large random scatter in the length data due to the dimness of the flame tails, there is a fluctuation in the lengths of some of the flames.

CHAPTER IV

CONCLUSION

Qualitative descriptions of flame shape and color and quantitative flame dimension measurements are used to investigate the effect of varying the velocity of the sample and the mole fraction of oxygen in the surrounding atmosphere on the very weak flames established above a solid fuel in a low speed forced flow. These two types of results will be combined to give as complete a description of these flames as possible with the present data. The front of the flame is the brightest and most clearly defined part of the flame, so the flame dimensions taken from the front of the flame are more accurate than the length measurements taken from the tail of the flame, which was very dim and seemed to fluctuate. The flame dimensions taken from the front of the flame -- stand off distance, width, and thickness -- showed regular and reasonable trends with varying velocity and oxygen concentration. From this evidence it is concluded that the phenomena at the front of the flame are repeatable, while those in the tail of the flame are not.

None of the flames reached steady state so to compare results from different tests, some assumptions

must be made. When comparing flame dimensions it is assumed that if both the value and the rate of increase of a particular dimension are larger for one flame than for another, then the steady state flames will show the same trend. Using this assumption it is found that as the velocity is lowered the flame moves farther from the fuel surface. Both the stand off distance and the flame width increase with decreasing velocity. These trends are reversed when the oxygen mole fraction is lowered. The stand off distance and flame width decrease with lowered oxygen concentration. The flame shape ratio, defined as the ratio of the flame width at the leading edge of the sample to the stand off distance, was found to be insensitive to changes in velocity and oxygen concentration. These trends compare well with those from calculations by T'ien [5] and Chen [7,8,9]. However, these models predict the same general trends for the cases with and without surface radiation. Because there are only six data points and because the flames do not reach steady state, there is no way to tell whether this data match the calculations that include radiation any better than those that do not. So, while the most basic of trends can be deduced from the flame dimension data, no conclusion can be drawn about the existence of a low

speed extinction limit.

While the trends in the flame dimension data are not unusual, the magnitude of the flame dimensions are. The smallest stand off distance observed was 3.4$\pm$ .7 mm and the largest stand off distance observed was 8.4$\pm$ .7 mm and in all cases the stand off distance was growing at the end of the test. The flame thicknesses were about 1 or 2 millimeters. These flames are much farther from the fuel surface and much thicker than the vast majority of flames observed in normal gravity. These large stand off distances mean that the heat flux to the fuel surface is very low and that the flames are very weak.

Using a simple soot formation model some conclusions about flame temperature can be drawn from the qualitative flame color data. More soot formed at the tests with the higher velocities and oxygen concentrations. While lowering the velocity increases the gas residence time, aiding soot formation, it is observed that less soot forms as the velocity is lowered. These flames, therefore, must be cooler than those at higher velocities. This conclusion is only for the transient flames. Soot formation, when it occurred, did so in a regular manner, starting with an all blue flame. It is possible that the flames at the

lower velocities are blue simply because they have not had time to develop soot yet. No conclusions can be drawn about the steady state temperatures from this data. The steady state calculations by T'ien [5] and Chen [7,8] predict that when surface radiation is neglected the flame temperature is independent of velocity, while for the case with radiation the flame temperature falls as the low speed limit is approached. Again the present data cannot differentiate between the two cases.

There are several ways that future work can improve on the work done here. The biggest improvement would simply be to obtain more data. Using a more reliable ignition method will make this possible. A smaller igniter that moves with the sample will be more reliable than the large stationary igniter used here. Using a thermocouple would be much more reliable than estimating temperature based on the flame color. The flame dimension data could be improved by focusing the camera on a smaller area and thereby improving the resolution of the picture. Finally, the single biggest improvement would be to obtain more time at low gravity.

The major accomplishment of this work is in providing a base for future work. Improved equipment

design is only one way future work will benefit from this project. Several new topics of research are suggested by these results. Because the soot forms very slowly and in a regular manner, these flames might be used to study soot formation. Also, since these flames develop so slowly, they offer a good opportunity to investigate transient flame behavior. Finally, this work provides a good starting point for any further investigations into the low speed extinction limit.

REFERENCES

1. Kimzey,J. H., Downs, W. R., Eldred, C. H., and Norris, C. W., "Flammability in Zero-Gravity Environment," NASA TR R-246 (1966).

2. Andracchio,C. R. and Cochran, T. H., "Gravity Effects on Flame Spreading over Solid Surfaces," NASA TN D-8228 (1976).

3. Kumagai, S. and Isoda, H., "Combustion of Free Fuel Droplets in a Freely Falling Chamber," Thirteenth Symposium (International) on Combustion, p. 779-785 (1970).

4. Okajima, S. and Kumagai, S.,"Further Investigations of Combustion of Free Droplets in a Freely Falling Chamber Including Moving Droplets," Fifteenth Symposium (International) on Combustion, p. 401-407 (1974).

5. T'ien, J. S., "Diffusion Flame Extinction at Small Stretch Rates: The Mechanism of Radiative Heat Loss," Combustion and Flame, 65,pp. 31-34 (1986).

6. Foutch, D. W. and T'ien, J. S., "Extinction of a Stagnation Point Flame at Reduced Gravity," presented at the Central States Section / Combustion Institute Meeting, May 5-6 (1986).

7. Chen, C. and T'ien, J. S., "Diffusion Flame Stabilization at the Leading Edge of a Fuel Plate, " Combustion Science and Technology, Vol. 50, # 4-6, p. 283 (1986).

8. Chen, C., "Diffusion Flame Extinction in Slow Convective Flow Under Microgravity Environment," NASA TM 88799 (1986).

9. Chen, C., personal communication, August, 1986.

10. Kanury, M. A., Introduction to Combustion Phenomena, Gordon and Breach Science Publishers, p. 143 (1982).

11. Sohrab, S. H., Williams, F. A., "Extinction of Diffusion Flames Adjacent to Flat Surfaces of Burning Polymers," J. of Polymer Science: Polymer Chemistry Edition, Vol. 19, p. 2955-2976 (1981).

12. Hirano, T., Noreikis, S. E., and Waterman, T. E., "Measured Velocity and Temperature Profiles Near Flames Spreading over a Thin Combustible Solid," Combustion and Flame, 23,pp 83-96 (1974).

13. Campbell, A. S., "Some Burning Characteristics of Filter Paper," Combustion Science and Technology, Vol 3, p. 103-120 (1971).

14. Olson, S. L. and T'ien, J. S., "A Theoretical Analysis of the Extinction Limits of a Methane-Air Opposed-Jet Diffusion Flame in the Absence of Buoyancy-Induced Flows," presented at the Central States Section / Combustion Institute Meeting, May 5-6 (1986).

15. Chu, L., "Upward Spreading Flames over Paper Samples," Thesis, Case Western Reserve University, FTAS/TR-78-139 (1978).

Properties of Nonadecane

Chemical formula	:	$C_{19}H_{40}$
Specific Gravity	:	.7857 (at 4 C)
Melting Point	:	31.4 C
Boiling Point	:	336.2 C
Heat of Vaporisation	:	142.1 J/gr
Heat of Combustion	:	12,643 kJ/mole
Vapor Pressure	:	1.46 kPa (at 186 C)
		13.3 kPa (at 248 C)

Table 1. Properties of Nonadecane

Properties of Fiberfrax

Continuous use limit	:	1260 C
Melting Point	:	1790 C
Density	:	160-192 kg/m^3
Specific Heat	:	1130 J/kg (at 1093 C)
Thermal Conductivity	:	.072 W/m- C (at 427 C)
		.140 W/m- C (at 871 C)
Reflectivity	:	.2 (at 427 C)
		.5 (at 800 C)

Table 2. Properties of Fiberfrax

Test Conditions

Data point #	Velocity	Oxygen Mole Fraction
1*	3.7 cm/s	.19
2*	1.1 cm/s	.18
3	2.4 cm/s	.18
4	3.6 cm/s	.18
5	6.3 cm/s	.18
6*	6.2 cm/s	.17
7*	0.0 cm/s	.16
8	1.4 cm/s	.16
9*	1.8 cm/s	.16
10a*	3.8 cm/s	.16
10b*	3.7 cm/s	.16
11	6.1 cm/s	.16
12	2.9 cm/s	.15

*flame was not two dimensional

Table 3. Test Conditons

ORIGINAL PAGE IS
OF POOR QUALITY

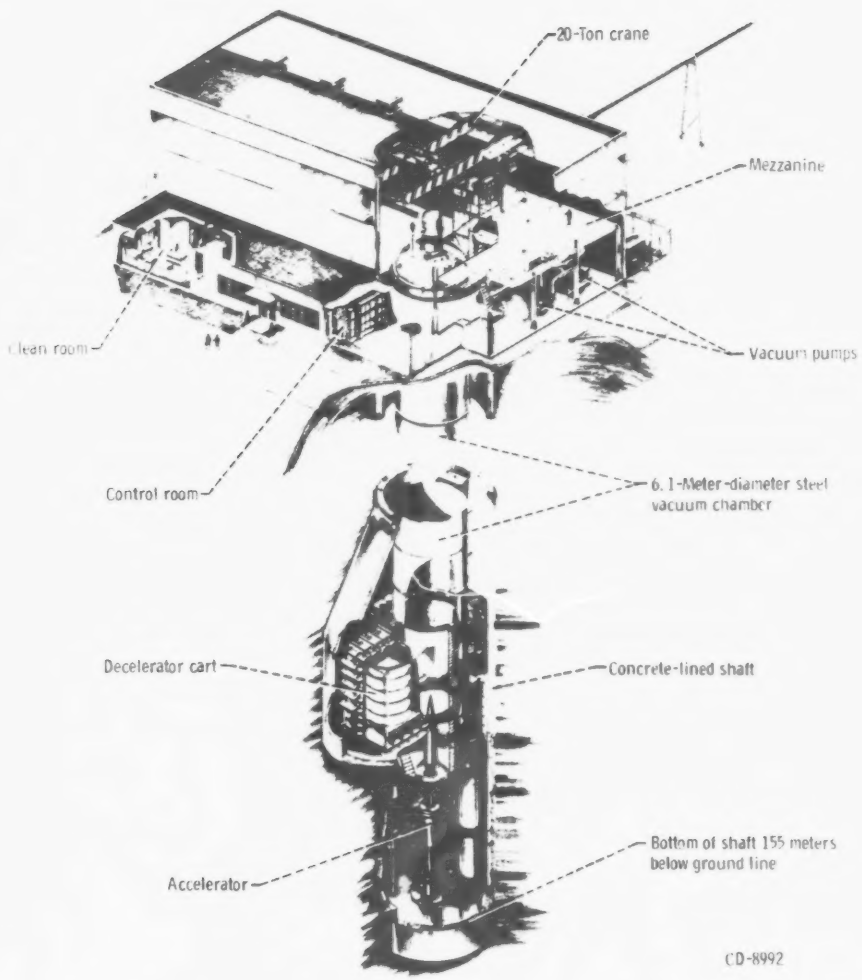

Figure 1. Schematic of the Zero Gravity Facility.

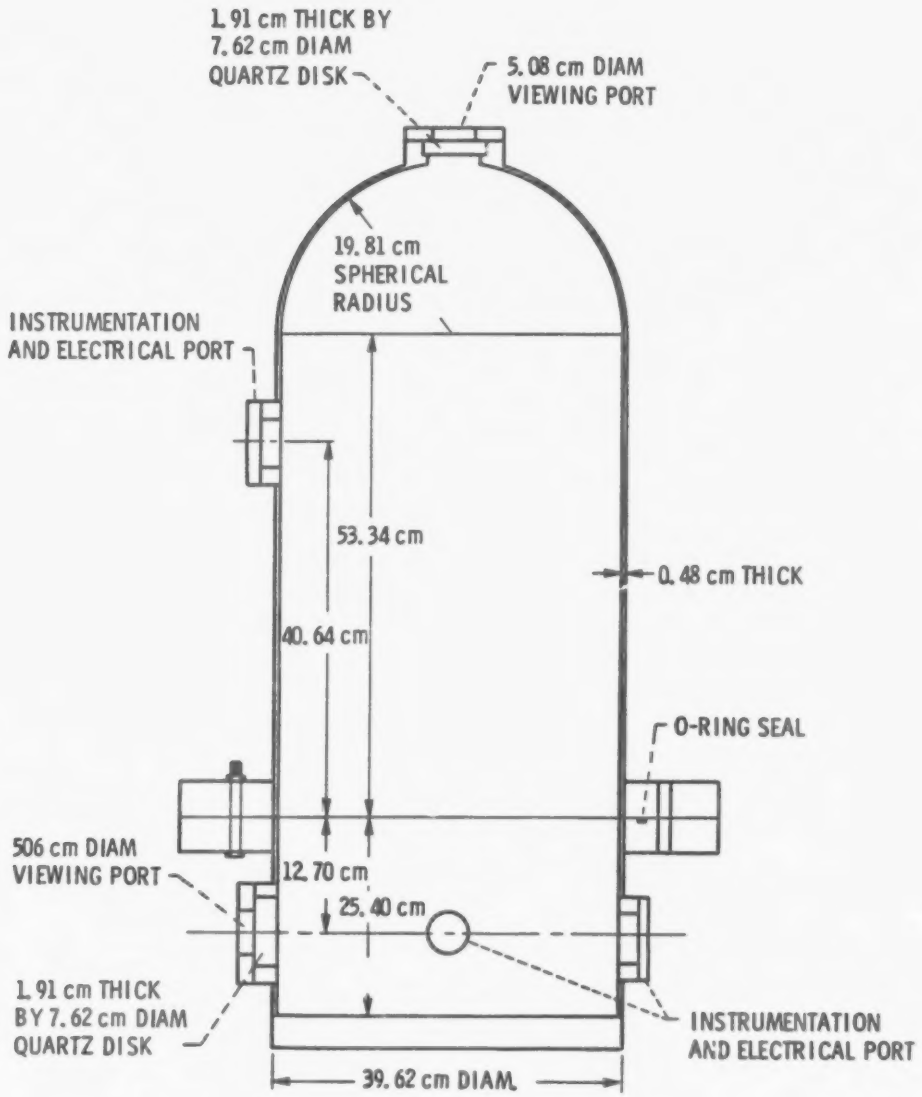

Figure 2. Cross-Sectional Schematic of Combustion Chamber

ORIGINAL PAGE IS
OF POOR QUALITY

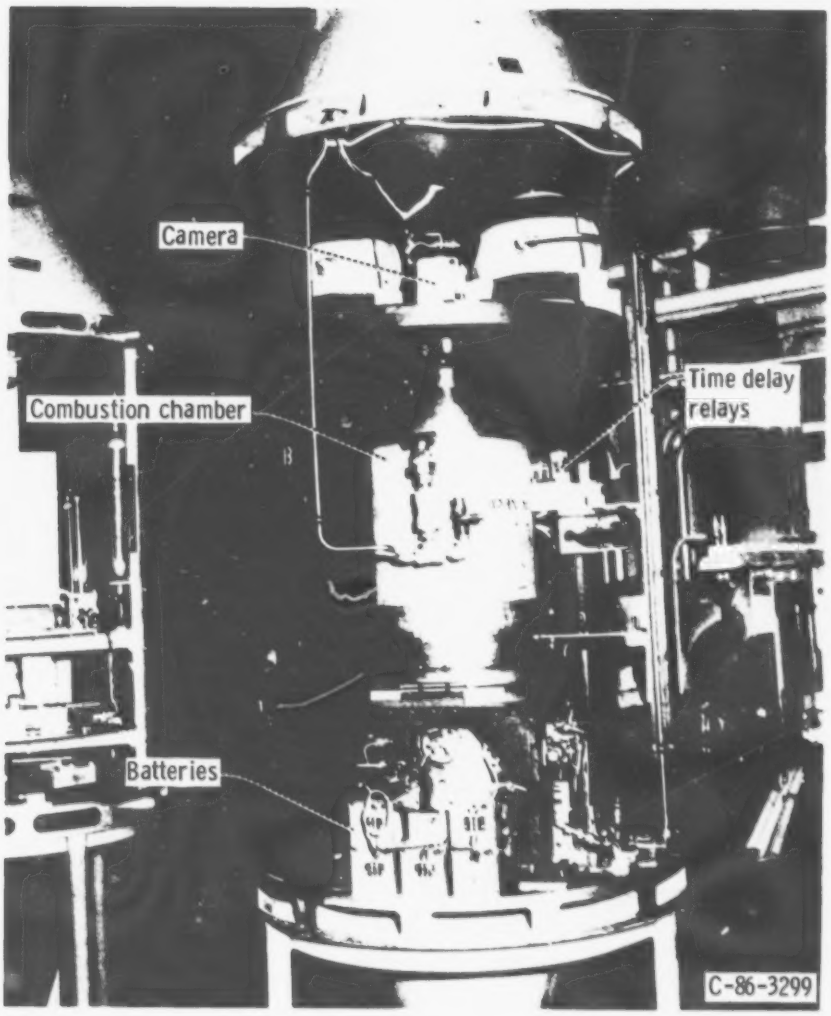

Figure 3. Combustion Chamber and Drop Package.

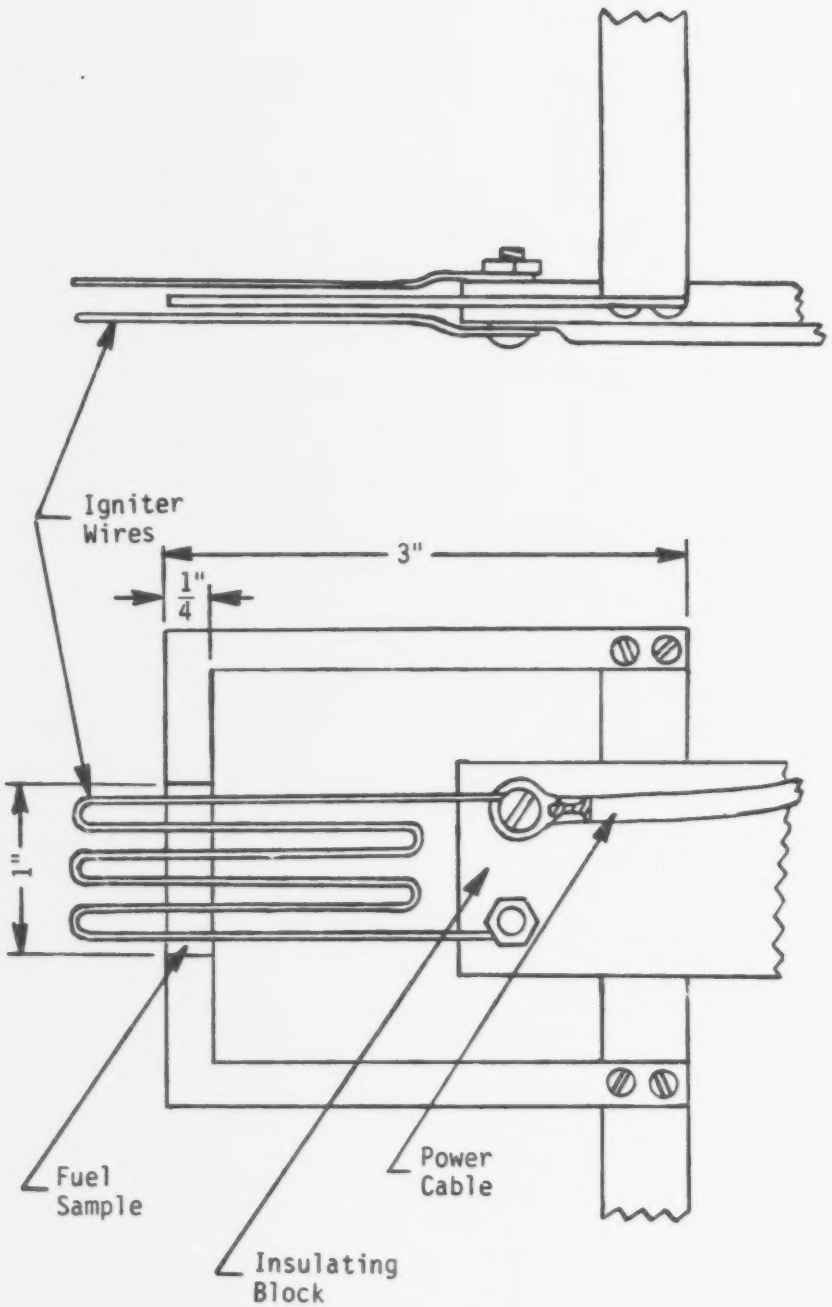

Figure 4. Position of Fuel Sample, Sample Holder, and Igniter Wires

ORIGINAL PAGE IS
OF POOR QUALITY

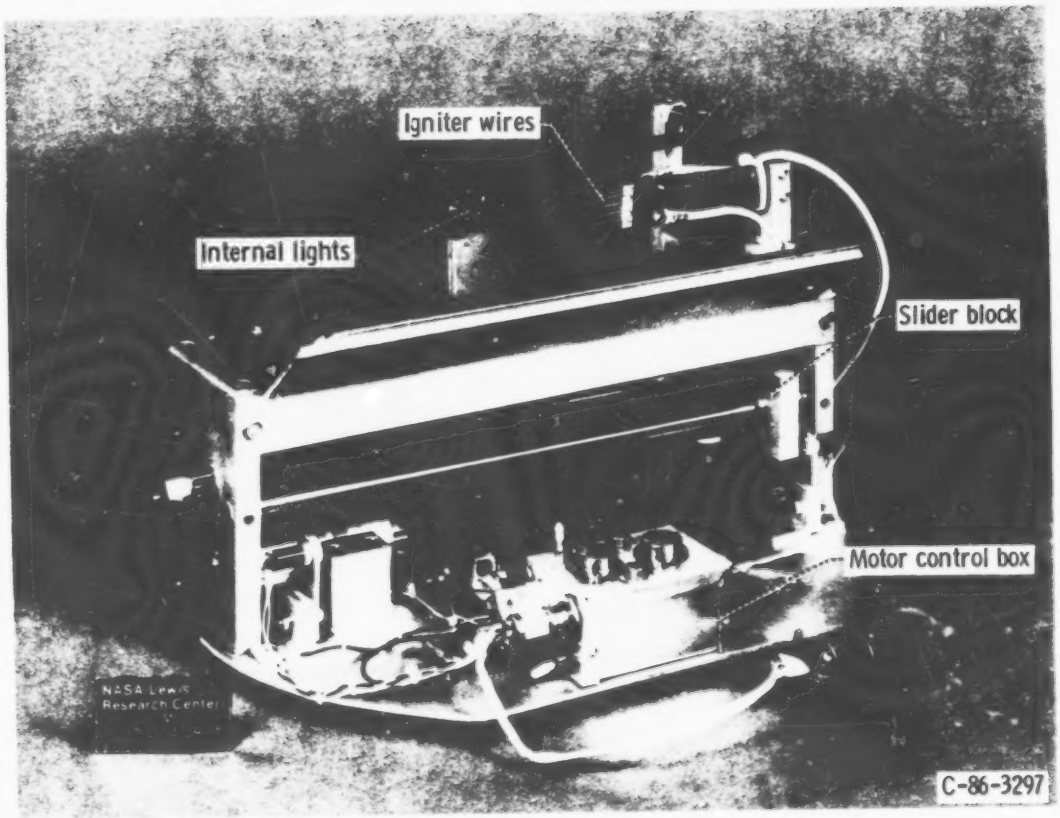

Figure 5a. Drive Mechanism and Ignition System.

ORIGINAL PAGE IS
OF POOR QUALITY

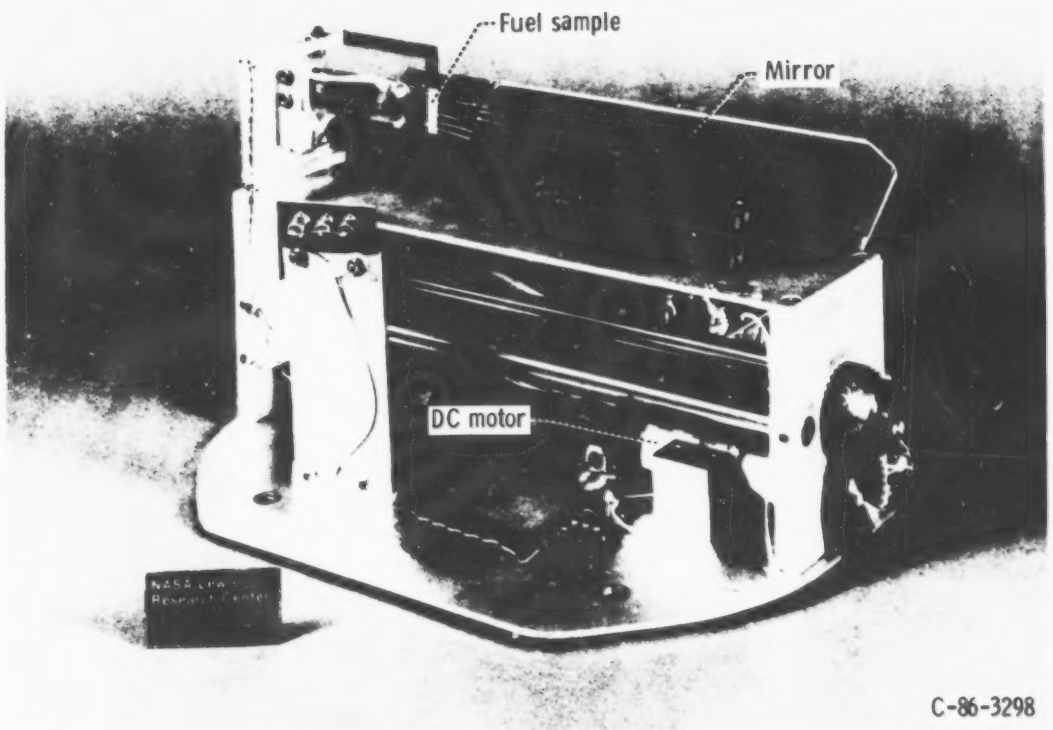

Figure 5b. Drive Mechanism and Ignition System.

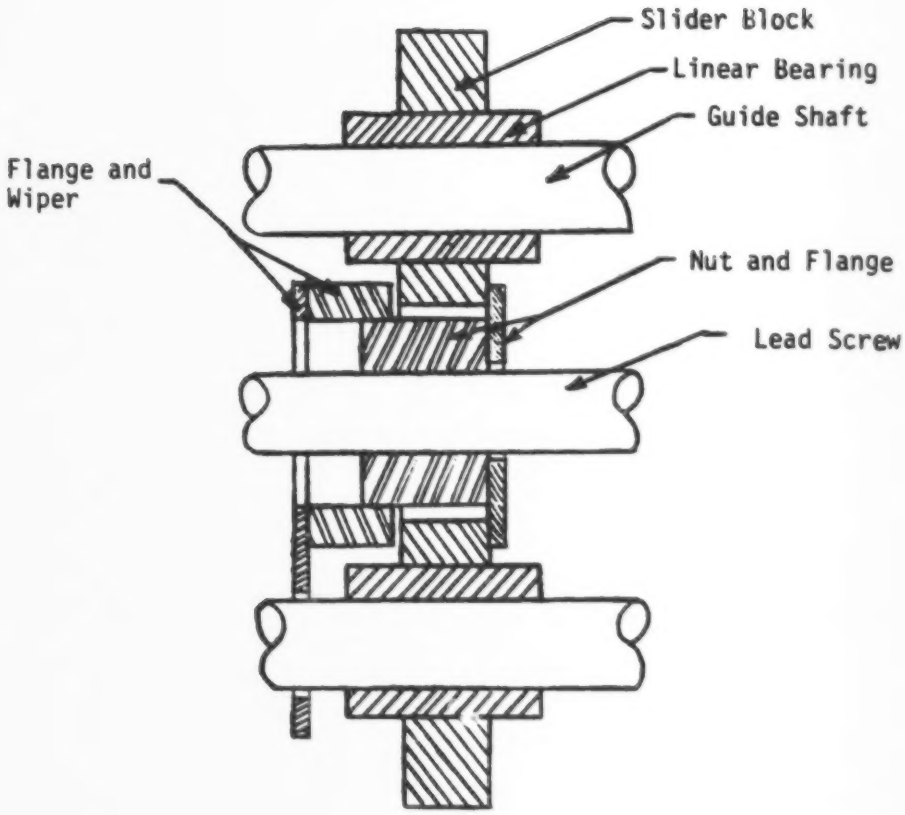

Figure 6. Section View of Slider Block and Nut

ORIGINAL PAGE
COLOR PHOTOGRAPH

ORIGINAL PAGE
COLOR PHOTOGRAPH

Flame Appearance at End of Drop

plan view edge view

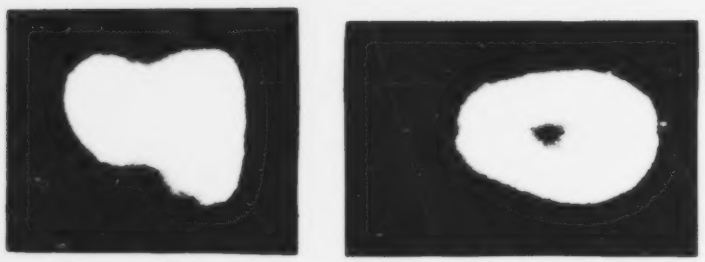

#5

V=6.3 cm/s

X_{O_2}=.18

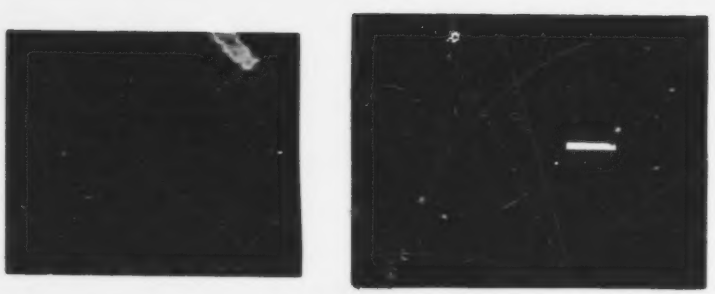

#4

V=3.6 cm/s

X_{O_2}=.18

#3

V=2.4 cm/s

X_{O_2}=.18

Figure 7. Flame Appearance at End of Drop

ORIGINAL PAGE IS
OF POOR QUALITY

Flame Appearance at End of Drop

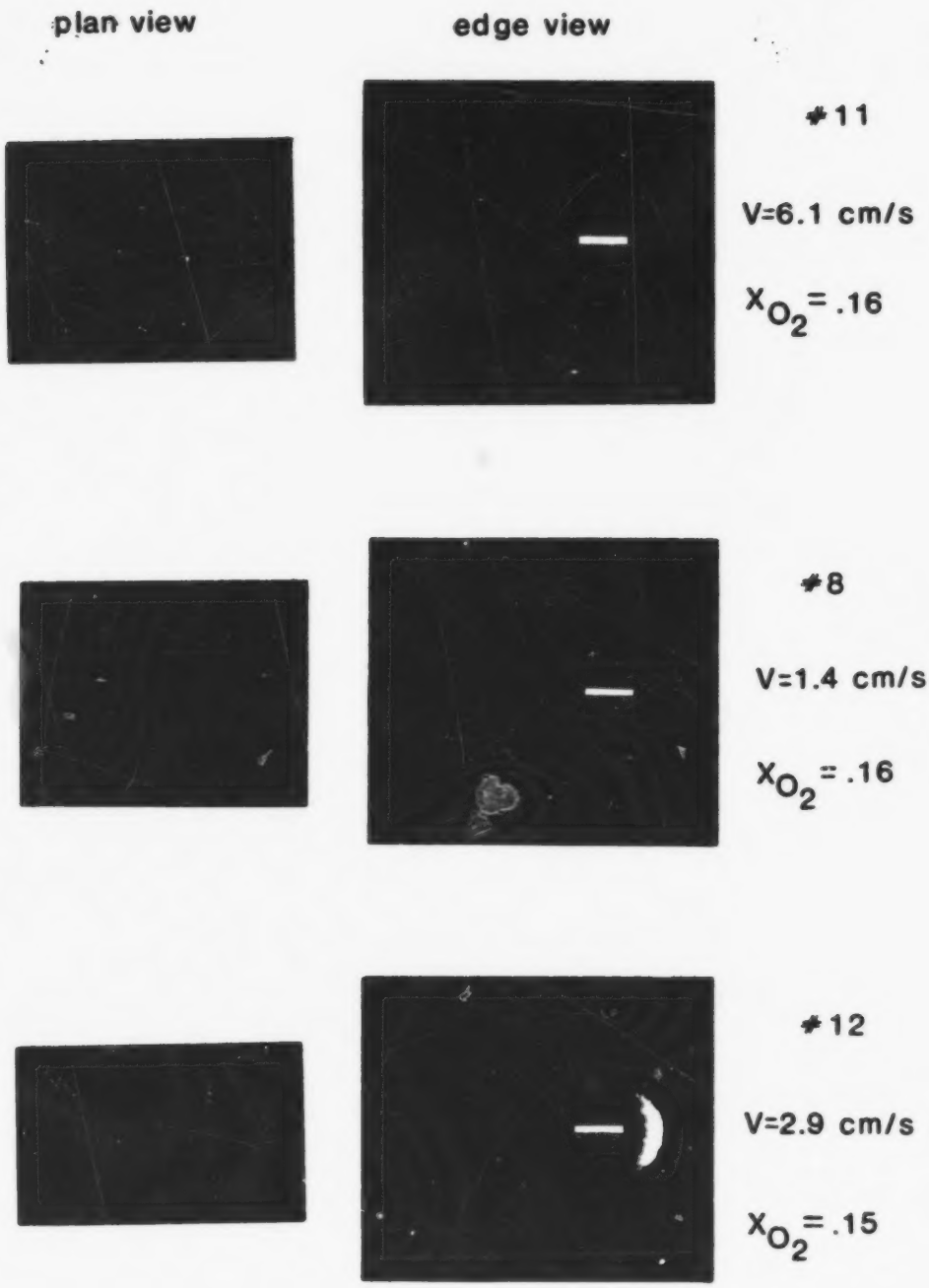

Figure 7, cont'd. Flame Appearance at End of Drop

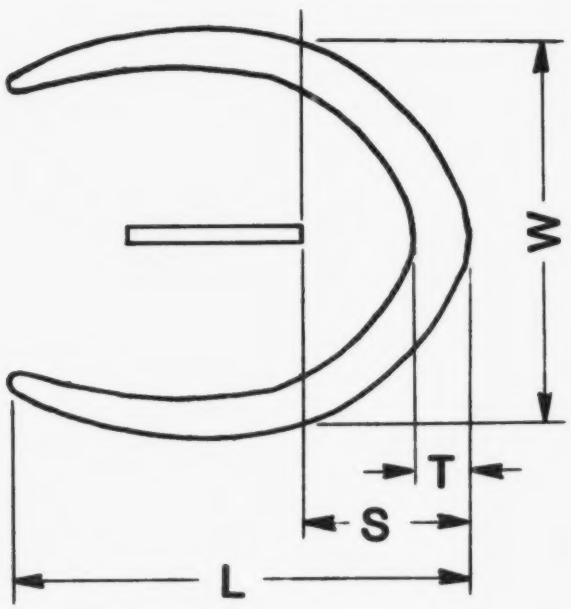

Figure 8. Flame Dimensions

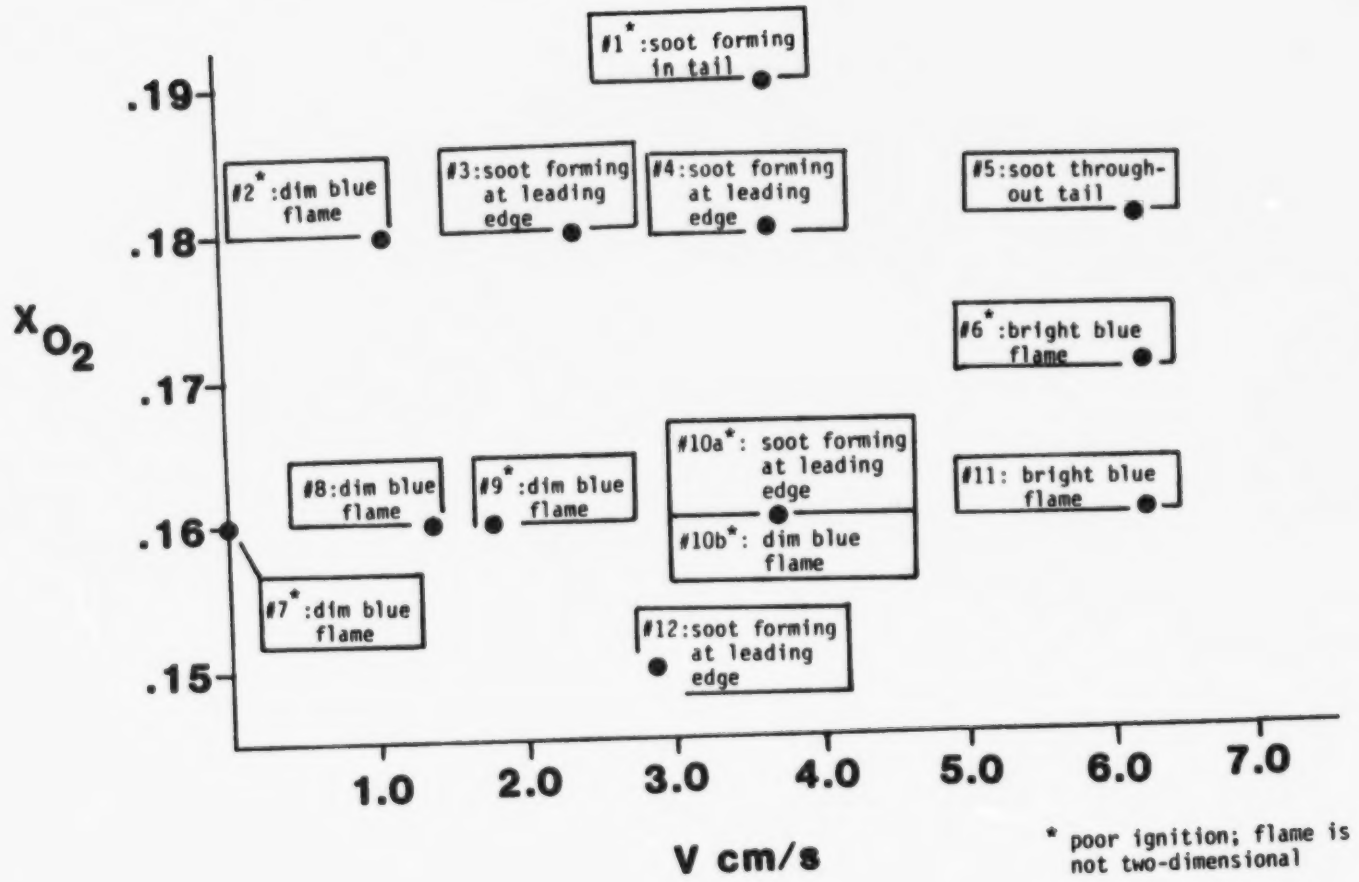

Figure 9. Variation of Flame Appearance with V and X_{O_2}.

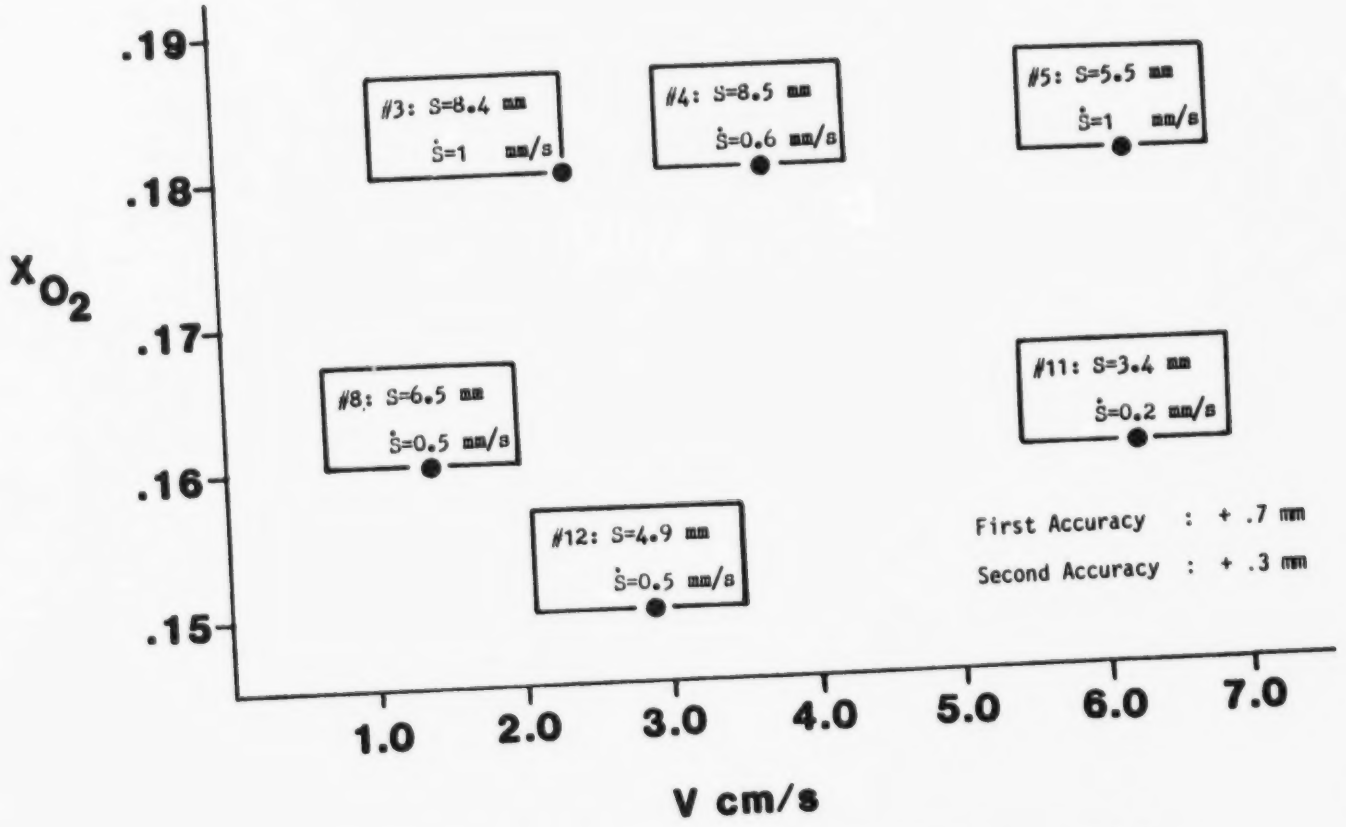

Figure 10. Variation of Stand Off Distance with V and X_{O_2}

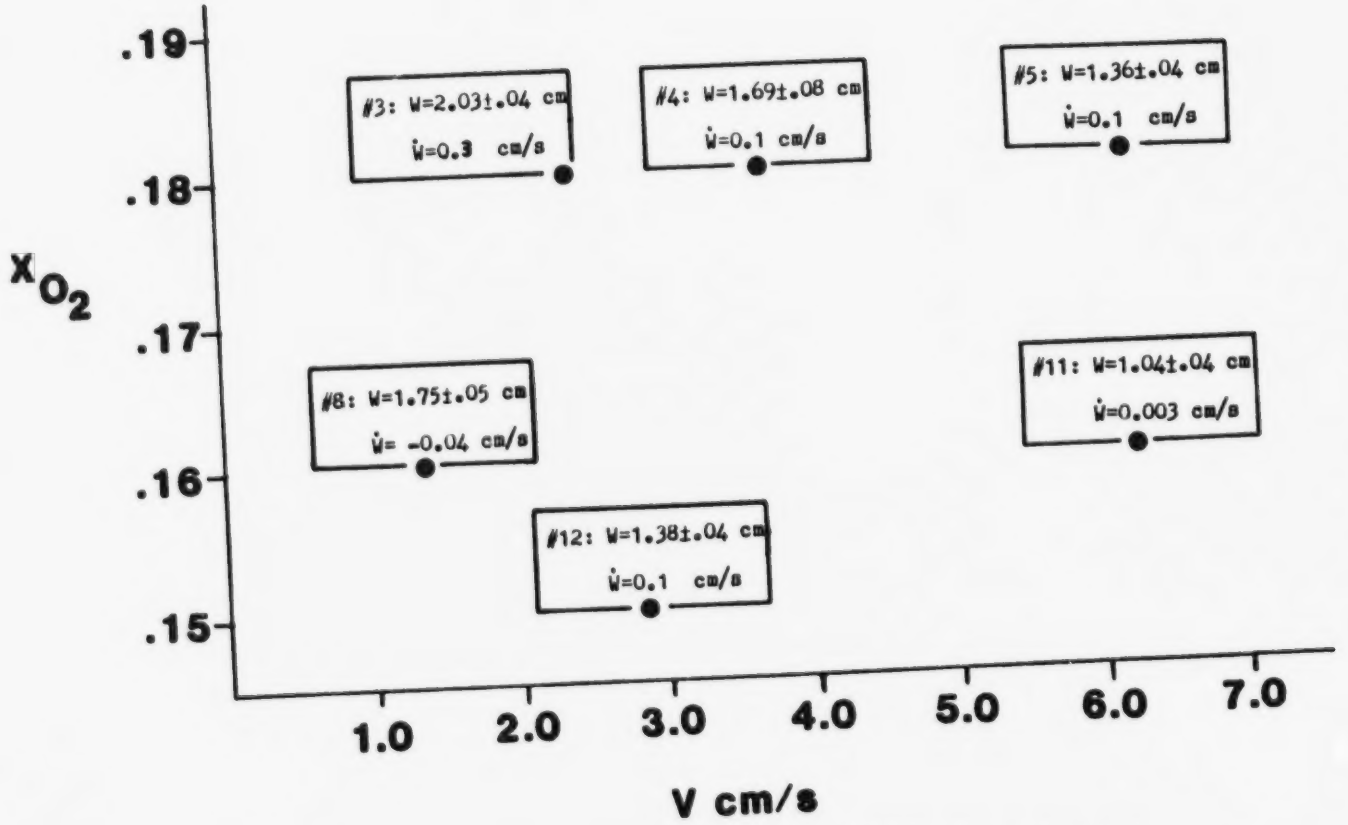

Figure 11. Variation of Flame Width with V and X_{O_2}

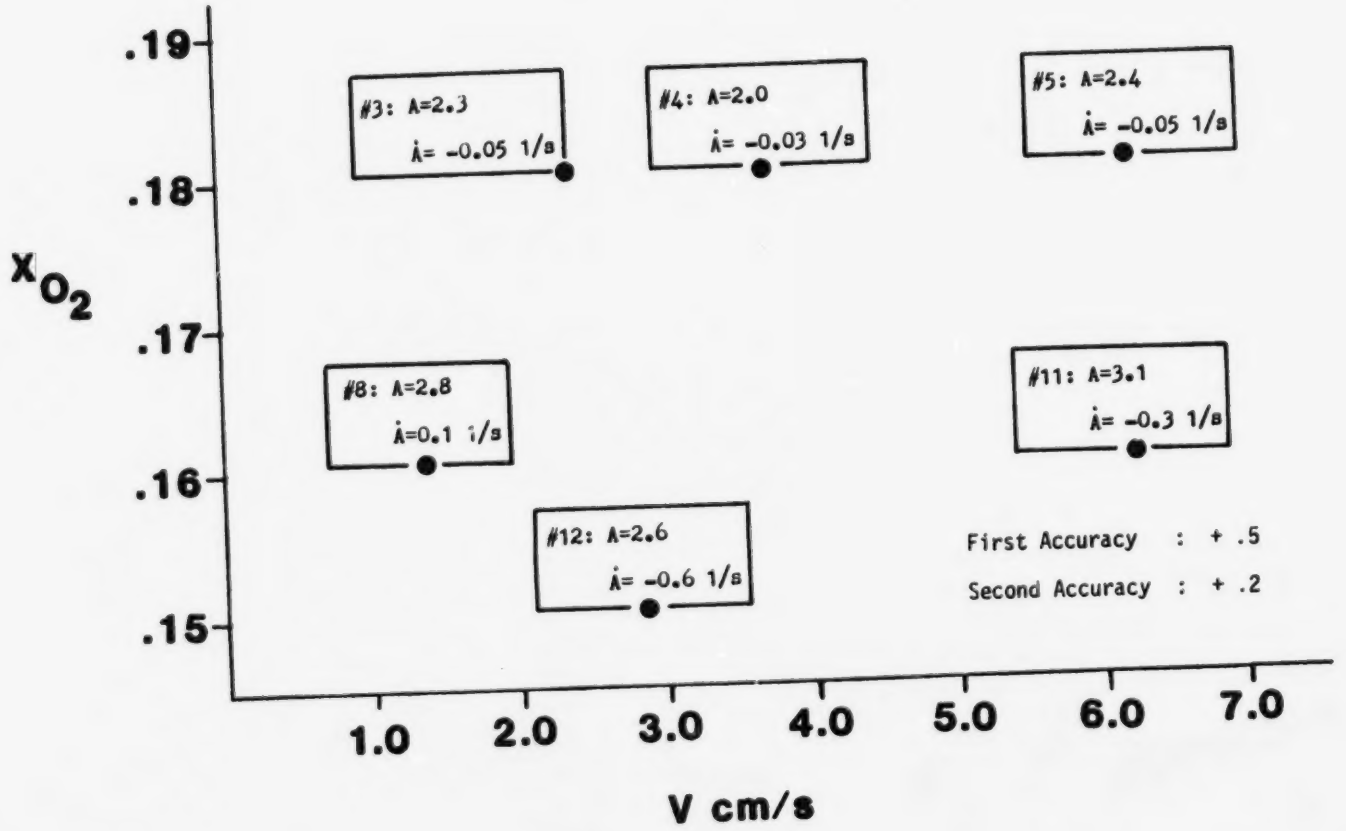

Figure 12. Variation of Flame Shape Ratio with V and X_{O_2}.

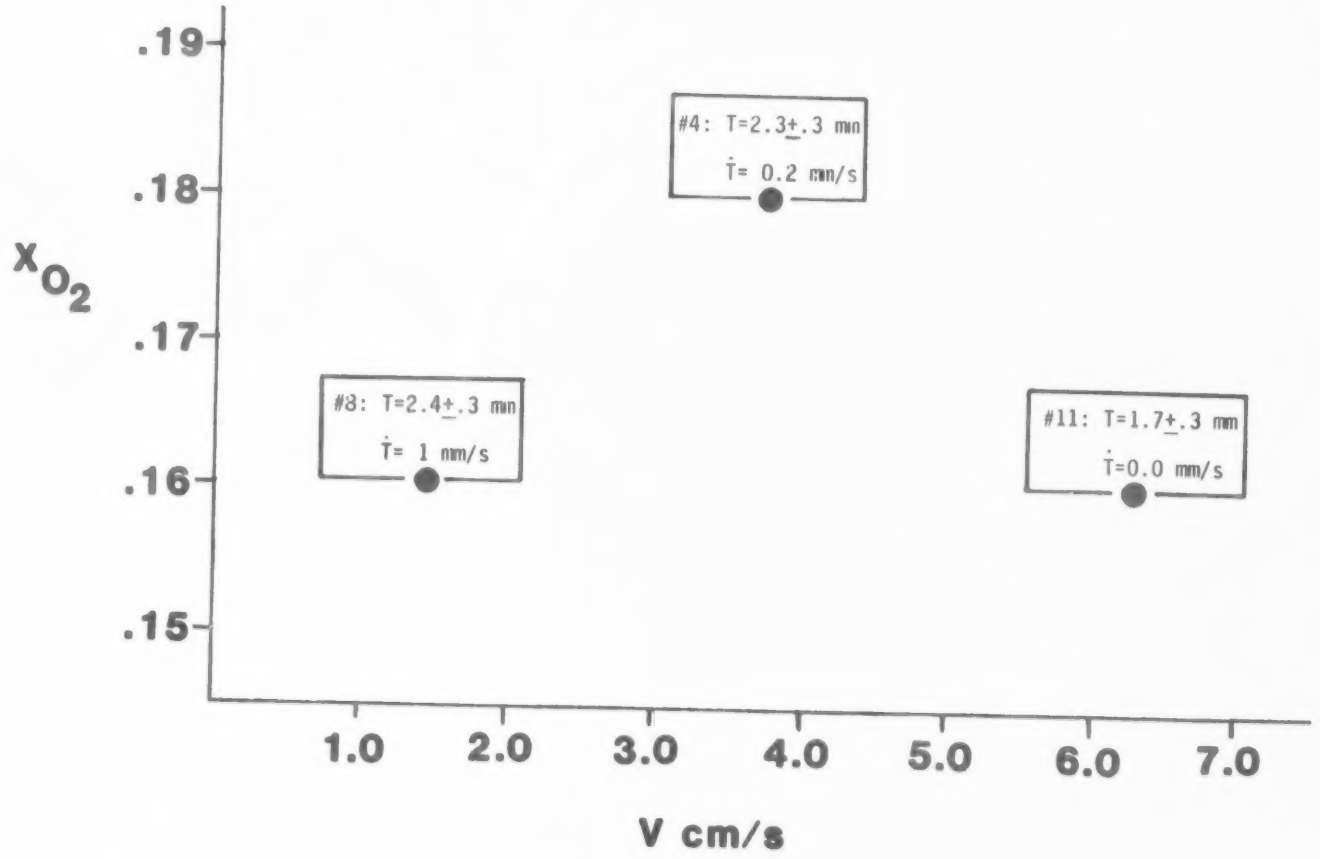

Figure 13. Variation of Flame Thickness with V and X_{O_2}

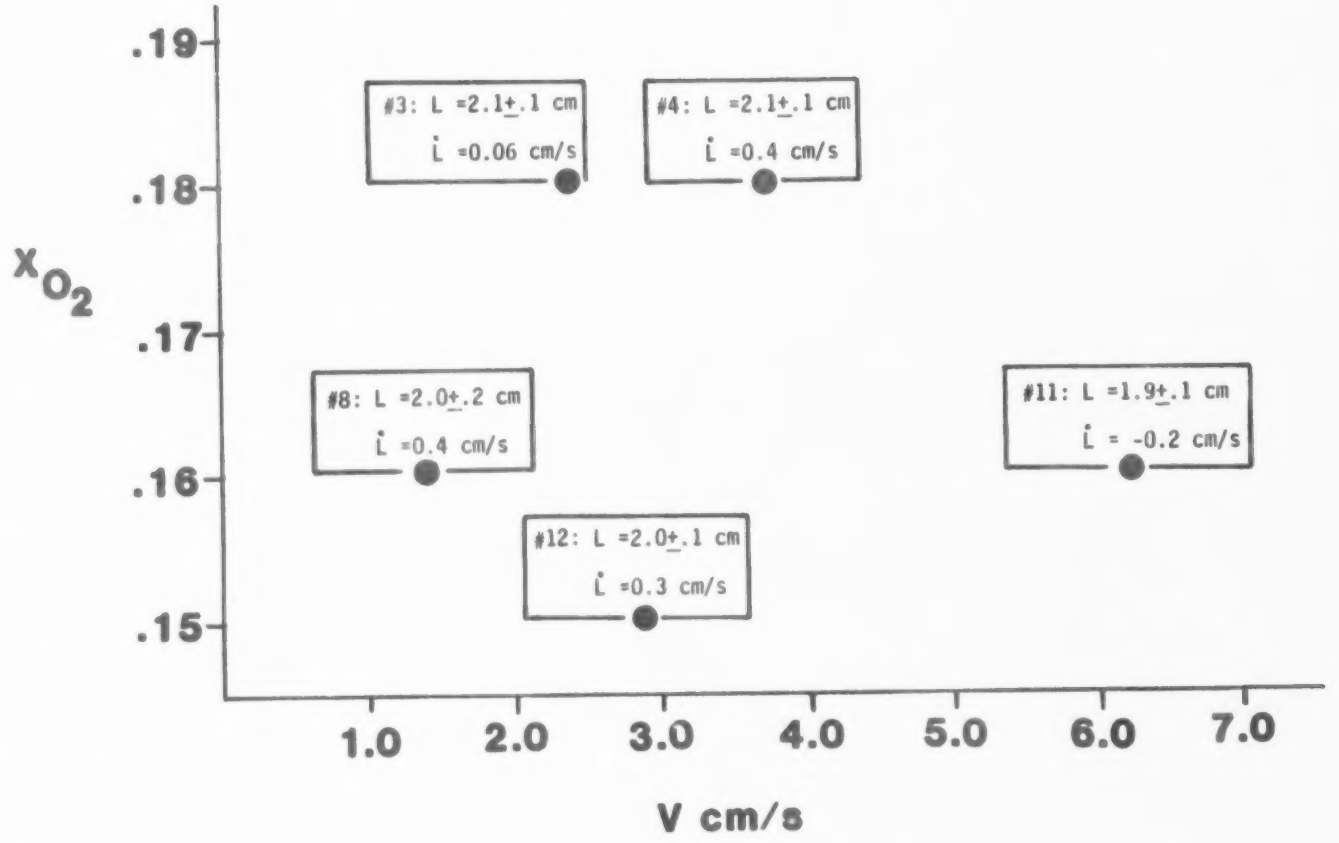

Figure 14. Variation of Flame Length with V and X_{O_2}.

APPENDIX A

ERROR ANALYSIS

A.1 Measurements from Film

The only raw data in this experiment is high speed color motion pictures. All of the flame data and velocity measurements are taken off of these films using a motion analyzer linked to a personal computer. The errors associated with this process will be discussed here.

The motion analyzer is equipped with a cursor. When the cursor is placed on the screen and the cursor button is pressed, the frame number and the x-y position of the cursor relative to a fixed-to-the screen origin are transmitted to the computer. In order to translate between the films and the physical world, the film data has to be calibrated. This is done by filming a scale marked in centimeters and determining the scaling factor between the motion analyzer coordinates and centimeters. It was found that there was a 2% variation in the apparent length of 1 cm for different locations in the field of view. This discrepancy is probably due to simple foreshortening. Because this 2% error is much less

than the other uncertainties in the measurements, no attempt is made to account for this foreshortening. The resulting scale factor is that 3.72 cm corresponds to 1.0 motion analyzer scale units. The calibration was only made in the direction of travel. It is assumed that the same relation holds in the direction perpindicular to the travel direction.

Because the sample is not visible during the experiment a red light emitting diode (LED) is fixed to the holder arm to indicate the position of the sample. This holder arm and the sample, however, are not the same distance from the camera and, as shown in Figure A.1, the apparent length between the LED and the sample depends on the position of the holder. Since the sample is far from the camera, theta is always less than .25 radians, so the relation between the actual length from the LED to the sample and the distorted length should be nearly linear for this small range of theta. This relationship is determined experimentally by making a film of the sample traveling across the field of view while the lights are on. Since the sample can now be seen, a calibration can be made between the position of the holder LED and the leading edge of the sample. A line is fit to the data using the least squares method, with the result:

XSAMP=2.18 + .940*XLED

where XSAMP and XLED are in the motion analyzer coordinates. The standard deviation of the data from this line is .017, which corresponds to .6 mm, or about 1% of the distance from the LED to the sample. This will be taken as the accuracy of this relation between XSAMP and XLED.

In addition to these errors, there are errors associated with the act of marking a point with the cursor. If a point is well defined, a sharp edge for example, the marking of that point is repeatable to .006 units in the motion analyzer coordinates, corresponding to .2 mm for this experiment. However, the dim blue flames do not have well defined points and measurements of the flame dimensions are much less repeatable. To estimate the accuracy of these measurements, data is taken from a single frame ten times. The accuracies given here are half of the spread between the highest and lowest values for each measurement:

holder position: $\pm$ .05 cm

thickness : $\pm$ .03 cm

flame length : $\pm$ .1 cm

flame width : $\pm$ .04 cm

stand off dist.: $\pm$ .03 cm

shape ratio : $\pm$ .2

In addition to error from marking the front of the flame, the stand off distance has an error due to the innaccuracy of the calibration discussed above. This error depends on the position of the holder. If two measurements are taken at nearly the same holder position, the error due to the calibration will be the same for each measurement and the two measurements can be compared to each other with the accuracy given above. If the measurements are taken at very different holder positions, an additional .06 cm of error is introduced because of the calibration. There are two cases where stand off distances can be compared with the above accuracy: when comparing neighboring points on stand off distance vs. time plots, as in Figure C.1, and when comparing final stand off distances for tests run at similar velocities, since the sample holder would have finished each test in the same position. A larger error must be used when comparing stand off distances at either end of the plot in Figure C.1 or final stand off distances run at different velocities. The same rules apply for the flame shape ratio, A.

Since the error from the calibration and the error from the measurement off the motion analyzer are

independent of each other, they add together as the square root of the sum of the squares. The following accuracies for the stand off distance and for the flame shape ratio reflect this additional error:

stand off distance: $\pm$ .7 mm

flame shape ratio : $\pm$ .5

The greater error will be called the "first accuracy" and the lesser error will be called the "second accuracy." To summarize the difference between the two accuracies for the stand off distance and the flame shape ratio, the second accuracy will be used to determine trends in the results in the last few moments of a test or between tests at similar velocities. The first accuracy will be used when determining trends between the beginning and the end of the drop and between tests at different velocities. Finally, the first accuracy, i.e. the larger error estimate, must be used when reporting the absolute magnitude of the stand off distance and the flame shape ratio.

A.2 Time

As the film runs through the camera a timing light flashes every 1/100th of a second, exposing a small portion of the film. The framing rate of the camera is calculated by counting the number of timing marks that

occur over a number of frames. The calculated framing rate is near 67 frames per second. It is now a simple matter to translate from the frame number provided by the motion analyzer into seconds. But it is not that simple due to an idiosyncrasy of the motion analyzer. It occaisionally and randomly miscounts the frames, at most leaving out about 1 frame in 25. So any time in this report can be as much as 4% low.

A.3 Velocity

The velocity was calculated from the slope of the least squares fit to the holder position vs. time data. The 2% error in the scaling factor between the motion analyzer units and the physical world, as discussed above, yields a 2% error in velocity measurement. The velocities given here have been corrected for the error in the time data described above, but a 2% uncertainty still exists. Since these two uncertainties are independent of each other, they combine to a total uncertainty of 3%.

A.4 Oxygen Mass Fraction

The gage used to measure the partial pressure of oxygen and the total pressure in the tank is accurate to .0125 psia, or 86 Pa. For a test at 16% O_2, the actual value of the oxygen mole fraction is 16 $\pm$.1 %.

A.5 Area Density of Fuel

The area density of the fuel in each sample was determined by measuring the mass, length, and width of each sample. An example calculation:

$$\text{area density} = \frac{(195.9 \pm .1 \text{ mg})}{[(3.84 \pm .03 \text{ cm}) * (.65 \pm .03 \text{ cm})]}$$

$$= 78 \pm 4 \text{ mg/cm2}.$$

The area density of Fiberfrax was determined in a similar fashion, except a piece 15 cm square was used to reduce the error. The result:

$$\text{area density of Fiberfrax} = 12.4 \pm .1 \text{ mg/cm2}.$$

The fuel area density in this case is therefore 68 ± 4 mg/cm2.

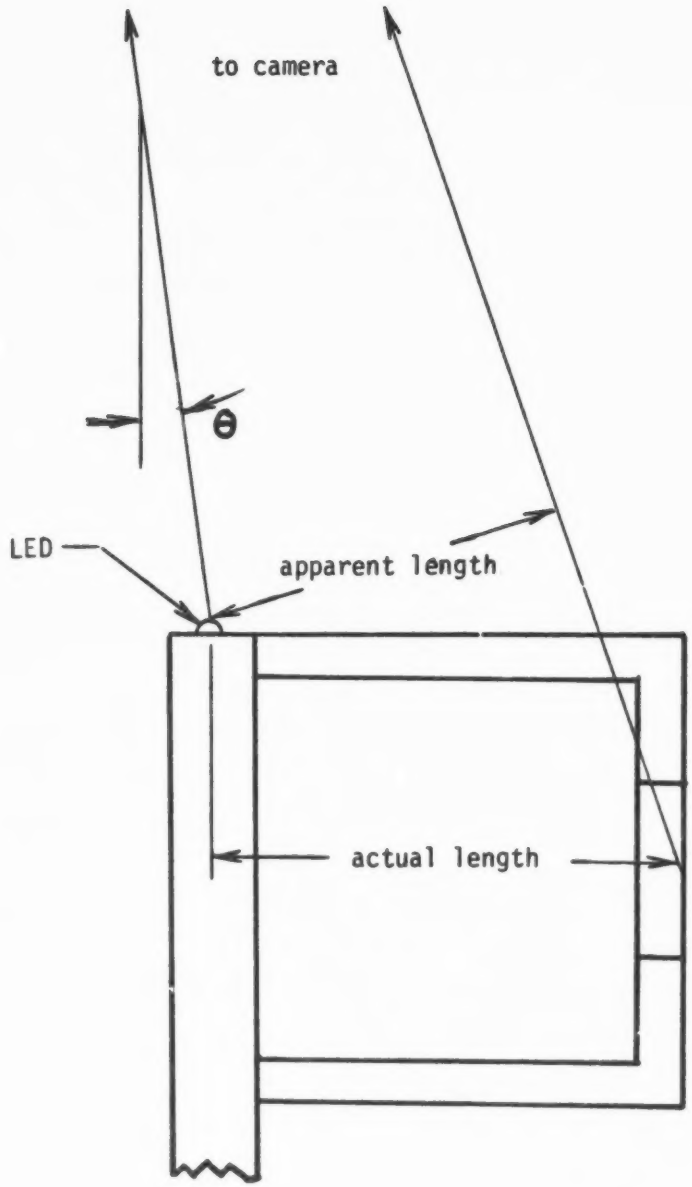

Figure A.1. Distortion of Length Between LED and Front of Sample.

APPENDIX B

DESCRIPTION OF TESTS

In this appendix the development of the flame in each test is described. Particular attention is given to the ignition of the sample, the flame shape and color, and whether the flame is two-dimensional. The B-8-xx series of numbers is used in the Zero Gravity Facility to keep track of the various experiments. This number is attached to the apparatus during a drop so the experiment number is visible on the films.

As explained in Appendix A, the times in these descriptions can be up to 4% low, due to an error in the motion analyzer. All the drops lasted 5.2 seconds, but the time measured with the motion analyzer varied somewhat from this. The motion analyzer times are used in the descriptions.

Data point 1, B-8-24:, V=3.7 cm/s, XO2=.19

The ignition wires get moderately bright. When the sample emerges from between the wires at t=2.5 sec., there is a small blue flame in front of the sample, but only on the top quarter of the plan view. This flame grows and spreads down the sample. At t=3.2 soot starts to form in the leading edge. The tail slowly lengthens, then at t=3.6 the flame propagates quickly

through a premixed region and encloses the sample with a blue reaction zone. The yellow soot zone continues to grow. In the plan view, the blue flame is across half the sample, with the center part of the blue region obscured by yellow soot. The flame continues to grow, moving farther from the fuel surface. The yellow region becomes thicker and spreads slowly downstream. At t=4.9 a small yellow region forms in the tail, right on top of the blue region in the tail. The drop ends at t=4.95 sec.

Data point 2, B-8-27, V=1.1 cm/s, XO2=.18

The ignition wires get very bright and the initial flame ball is very large. When the sample emerges from between the wires, the flame ball is about 2 cm from the front of the sample. The speed change from V=3.7 cm/s to V=1.1 cm/s occurs just after the sample emerges from the wires, at t=3.0 sec. The flame ball dims and stops expanding. The sample moves closer to the front of the flame ball. At t=4.6 a very dim blue flame becomes visible. The flame remains very large and very dim until the end of the drop, at t=5.1. No flame could be seen in the plan view. This flame may have been more of a remnant of the initial flame ball than a flame associated with the fuel sample.

Data point 3, B-8-11, V=2.4 cm/s, XO2=.18

The ignition wires get quite bright. The speed change occurs at t=1.5 seconds, while the sample has traveled about half the distance between the wires. When the sample emerges from the wires, the initial flame ball is about 1 cm away, with a flat front across the plan view. The sample moves into the ball of flame and a blue flame is established across the whole leading edge of the sample. The flame tail extends back at an angle, resembling a shock wave in front of a blunt body. The ends of the tails start to move toward the fuel surface. The flame is all blue and two dimensional. At t=4.5 the flame tail curves back toward the fuel surface and a dim yellow region is developing in the leading edge region. The yellow brightens, but at the end of the test, t=5.1, it is barely visible across the whole plan view.

Datapoint 4, B-8-9, V=3.6, XO2=.18

The ignition wires get very bright and the sample emerges from the wires with the flame ball about 1 cm away. The sample emerges from the flame ball with a dim blue flame in front of the sample, but only at the top of the plan view. At t=3.2 a flame front propagates very quickly from the top part of the tail

region down the back of the sample and around to the front of the bottom part of the sample. Now a closed, two dimensional, bright blue flame surrounds the sample. The flame grows slowly and the tail region gradually dims. At t=4.9 a dim region of yellow starts to form at the leading edge of the flame. At the end of the drop, t=5.2, the yellow has brightened somewhat, but is only barely visible in the plan view.

Data point 5, B-8-19, V=6.3 cm/s, XO2=.18

The wires get moderately bright. The speed change occurs when sample has traveled half the distance between the wires. At this time the initial flame ball is fairly small, about 1.5 cm in diameter. When the sample emerges from the wires, a small blue flame is established in front of the sample, but only at the top of the plan view. This blue flame grows slowly, and spreads across the sample. At t=3.0 a yellow region starts to form at the leading edge of the flame. The flame is about halfway across the sample now, but the tails of the flame do not extend downstream of the sample. The yellow gets brighter. It is starting at a point at the top of the plan view and spreading down the sample and downstream from there. At about t=3.3 a flame propagates through a premixed region in the rear of the flame to establish a closed blue flame in the

tail region. The yellow region in front of the sample has gotten quite thick. The yellow continues to spread across the sample and downstream. At t=3.7 a yellow region starts to form in the tail of the flame, and it forms at the top of the plan view first. By t=4.4 the yellow regions have merged, though in the plan view a dim region can be seen between them. The whole flame is now yellow; no blue can be seen. The tail of the flame lengthens throughout the remainder of the drop, which ends at t=5.1.

Data point 6, B-8-10, V=6.2 cm/s, XO2=.17

The ignition wires get quite bright. When the sample emerges from the initial flame ball, small blue flames are established in front of the sample at either end of the plan view. These flames lengthen and slowly spread across the sample. The double flame makes the edge view look strange. The bright blue flame continues to grow. By t=3.3 the two flames are starting to connect. At t=4.4 the view of the flame is obstructed. (In later drops the camera position is changed to prevent this obstruction.) Throughout the drop the center part of the flame never stabilizes. It seems to flicker -- sometimes the flame stretches across the whole sample and sometimes there

are two distinct flames at either end of the sample. For this reason the flame is not two-dimensional.

Data point 7, B-8-17, V=0.0, XO2=.16

The ignition wires get quite bright, but the initial flame ball does not get very big, .9 cm from sample when it emerges from between the wires. After it has emerged, a flame is established in front of the sample. It is stronger at the top, but does extend across the width of the sample. As soon as the sample stops at t=3.0 this flames dims and the plan view does not show a flame. The flame in the edge view does not extend downstream of the sample. The flame remains dim and slowly lengthens. At t=4.5 the flame propagates quickly through a premixed region in the tail. Now there is an asymmetric flame around 3/4 of the sample. The flame dims and by t=5.0 it has almost disappeared. But at t=5.1 the flame has brightened and can be seen in the same position as it was when the flame was first established in the tail region. The sample stopped just 1.4 cm from the end of the wire. The average speed in the three seconds before it stopped was 2.2 cm/s instead of the desired 3.7 cm/s. The sample moved very slowly at the beginning of the drop, then accelerated to 3.4 cm/s for the last one second before stopping. Since the sample was so close to the wire

and since the flame was asymmetric, this flame is not used in the flame dimension data.

Data point 8, B-8-15, V=1.4 cm/s, XO2=.16

The speed of the sample changes at the beginning. It starts very slowly, then speeds up. The ignition wires get fairly bright. As the sample emerges from between the wires, the initial flame ball is 1.1 cm away. There is a dim blue flame across the top half of the plan view when the sample emerges from the intial flame ball. When the speed changes, at t=3.0, the flame starts to dim and become shorter. The tails of the flame move away from the fuel sample, and slowly start to lengthen. The drop ends at t=5.2. By watching the plan view while the film is moving, a very, very dim flame can be seen across the whole sample. The flame is judged to be two-dimensional.

Data point 9, B-8-28, V=1.8 cm/s, XO2=.18

The ignition wires get very bright and the flame ball is very large. When the sample emerges from between the wires, it is 2.1 cm away. The flame ball stops expanding and starts to dim. The sample moves closer to the edge of the flame ball and at t=4.5 a dim blue flame is established in front of the sample. The flame is the same shape as the old flame ball and the

tails of the flame do not curve back to the surface. Nothing is visible in the plan view. The tails slowly move toward the fuel surface, but the drop ends at t=5.2. Again, the sample moved at the wrong speed, 1.8 cm/s instead of 2.5 cm/s.

Data point 10a, B-8-21, V=3.8 cm/s, XO2=.16

The ignition wires do not get very bright and the sample ignites on the side nearest the mirror first. When the sample emerges from the wires, the initial flame ball is .6 cm from the front of the sample. The flame nearly disappears when it emerges from the flame ball, then a small blue flame appears at the very top of the plan view. The flame is bright blue and slowly starts to grow, spreading downstream and across the sample. At t=4.5 a yellow region begins to form at the leading edge of the flame, and at the top of the plan view. When the drop ends at t=5.1 the flame is still only across half of the sample. The flame is judged to be three dimensional because it always seems to be affected by starting as a tiny flame at the top of the plan view. Because it started small and spread during the drop, it is not a two-dimensional flame.

Data point 10b, V=3.7 cm/s, XO2=.16

The igniter wires do not get very bright, though

the flame ball is fairly large. When the sample emerges from the wires, the flame ball is about 1 cm from the sample. No flame is visible after the sample emerges from the flame ball itself. Then a very dim blue flame forms in front of the sample, at the bottom part of the plan view. At t=3.6 a flame propagates through a premixed region, starting at the side of the sample away from the mirror and propagating around to the other side. It can also be seen to propagate in the tail region of the plan view, moving from bottom to top. When the propagation is finished, the flame in the tail disappears. When viewed at high speed, this whole process is visible as a flash of blue in the tail. This happens again at t=4.2 and again at t=4.8. In between these flashes the flame is very dim and only reaches a short distance downstream. The drop ends at t=5.2. Because the flame was only established at the bottom of the plan view and because these flashes occurred, the flame is judged to be three-dimensional.

Data point 11, B-8-12, V=6.1 cm/s, XO2=.16

Only the wire on the side of the sample away from the mirror gets bright, but it gets very, very bright. The flame ball starts on this side of the sample and then spreads around it. When the sample emerges from

the wires, the flame ball is about 2 cm away. The sample emerges from the flame ball and a small blue flame is established in front of the sample at the bottom of the plan view. At t=3.0 there are two trailing yellow regions that are the remains of the ignition transient. As these fade away the flame becomes all blue, extending downstream past the sample, with a small gap in the tail of the flame. Occasionally through the drop the tail looks as though it might be closed. The flame does not change much. It is bright blue and stretches across half the sample in the plan view. The front of the flame is straight in the plan view. Until the drop ends at t=5.2 the flame remains the same, not spreading across the sample. The flame is judged to be two-dimensional because the flame front is flat in the plan view and because it is not spreading at a visible rate across the sample.

Data point 12, B-8-18, V=2.9 cm/s, XO2=.15

The ignition wires get quite bright. When the sample emerges from between the wires, the flame ball is .9 cm away. The sample emerges from the flame ball with a small dim blue flame in front of the sample at the top of the plan view. The flame nearly surrounds the sample in the edge view. It is slowly spreading

across the sample. At t=4.2 very dim yellow appears in the leading edge. This yellow region grows brighter throughout the drop. It is only visible as a spot in the plan view. The drop ends at t=5.2. While the flame spreads across the sample during the drop, the spread is very slow and the flame front is flat, so the flame is judged to be two-dimensional.

APPENDIX C

TRANSIENT FLAME DIMENSION DATA

The following graphs are the results of the analysis of the films. The variation of the flame dimensions with time are shown. Two linear curve fits are given for most cases, one for all the data points, the other for approximately the last half second. These curvefits are found using the least squares method. The standard deviation is the standard deviation of the data from the line. In cases where an overall linear curve fit did not make sense, only the fit for the last half second is given.

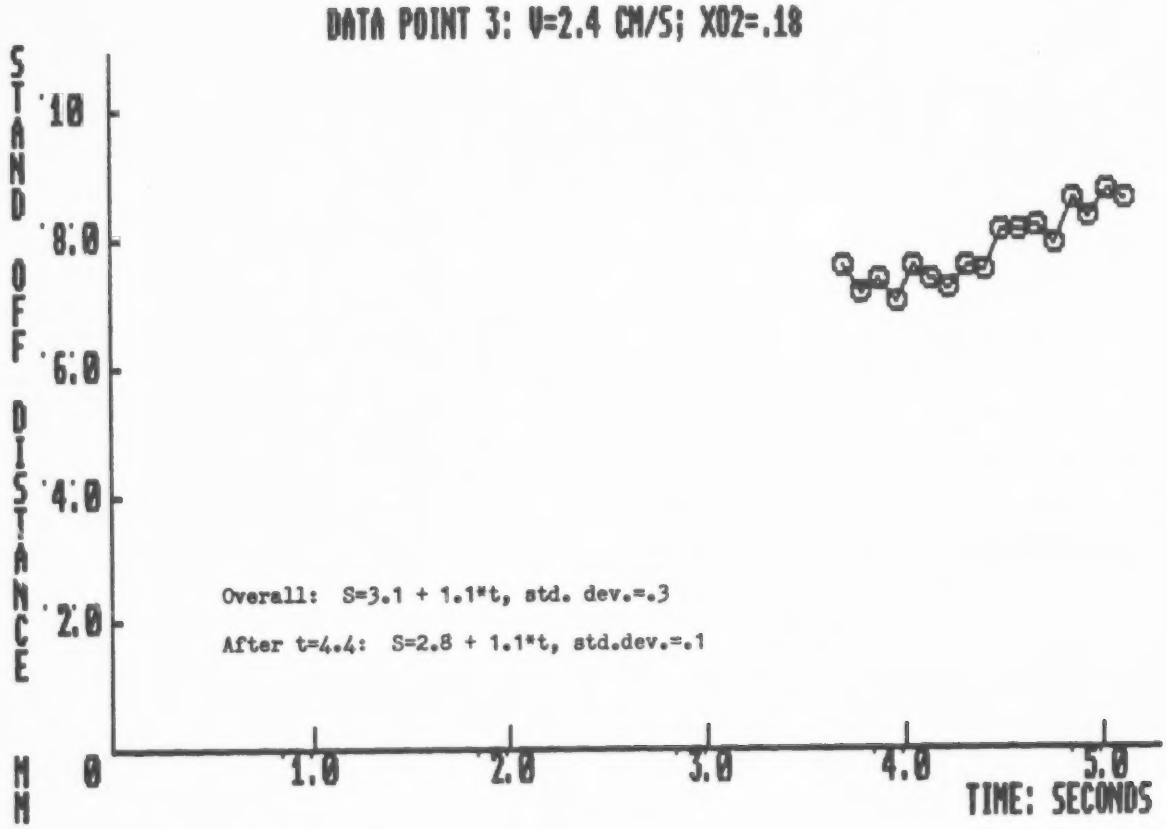

Figure C.1. Stand off distance versus time for data point 3.

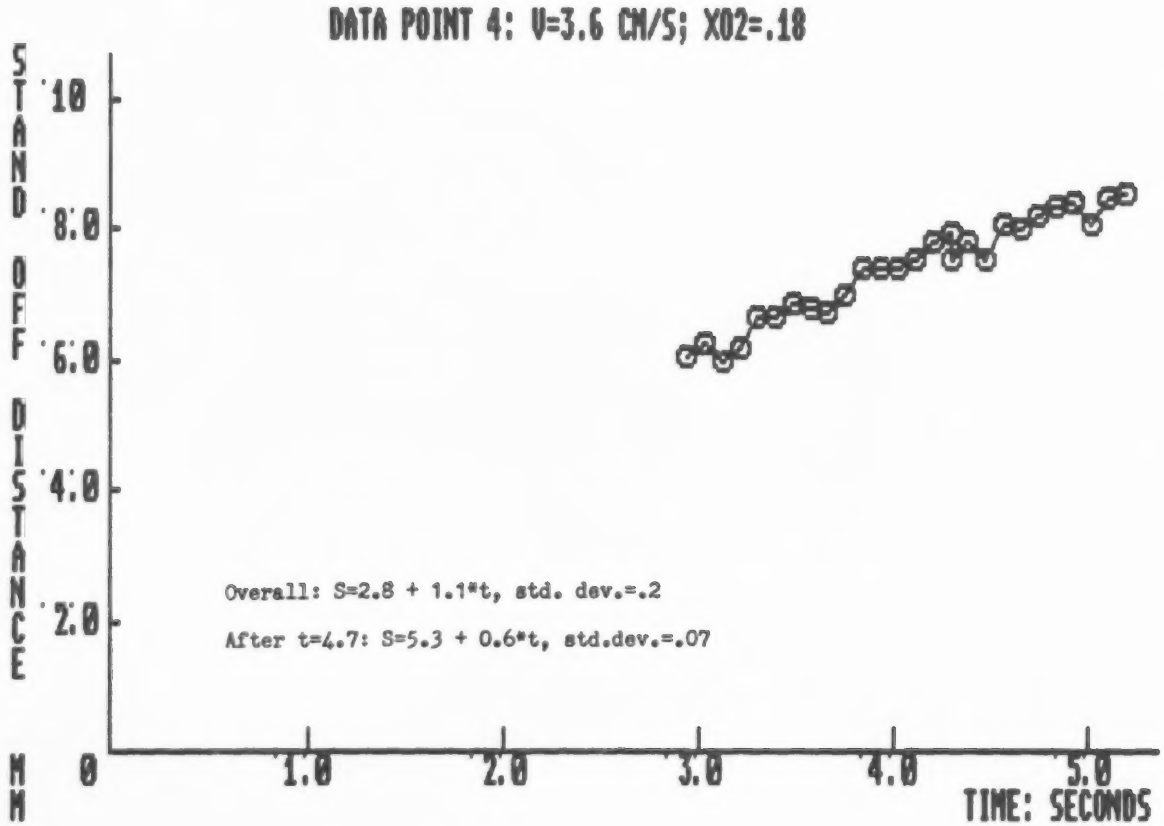

Figure C.2. Stand off distance versus time for data point 4.

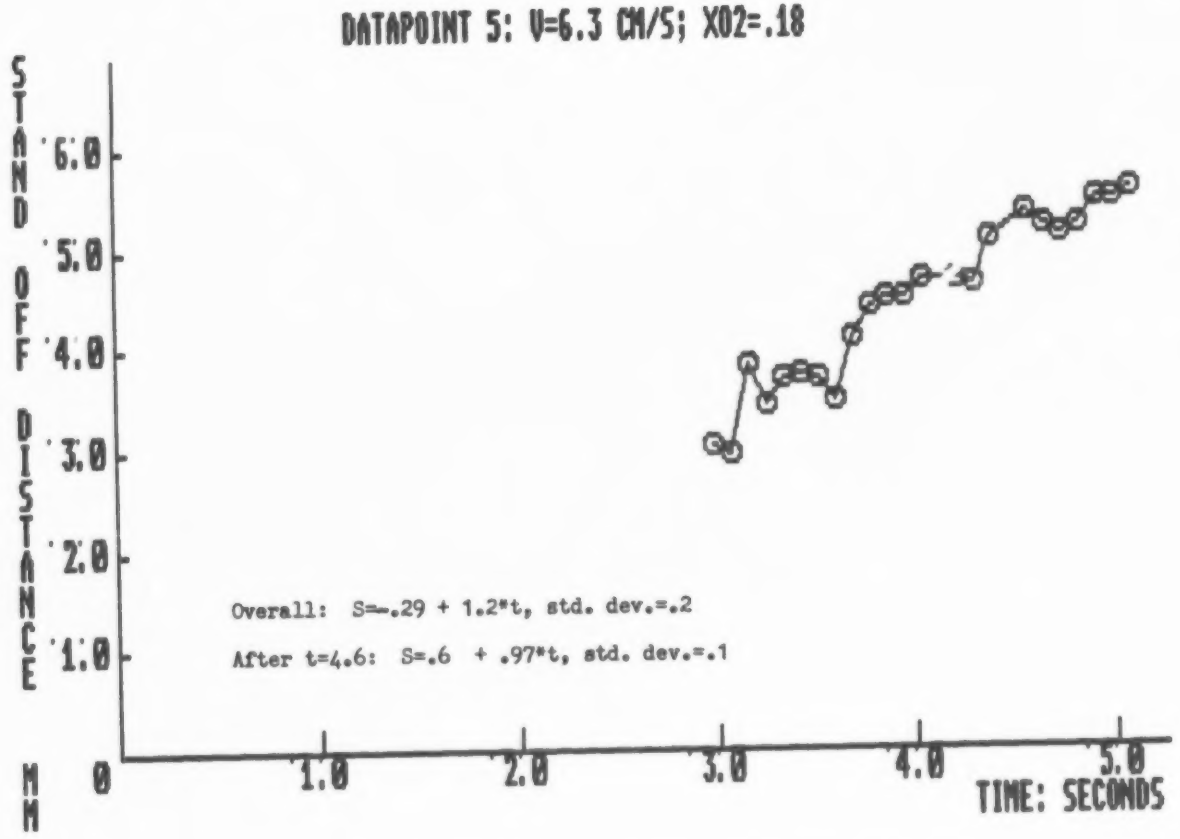

Figure C.3. Stand off distance versus time for data point 5.

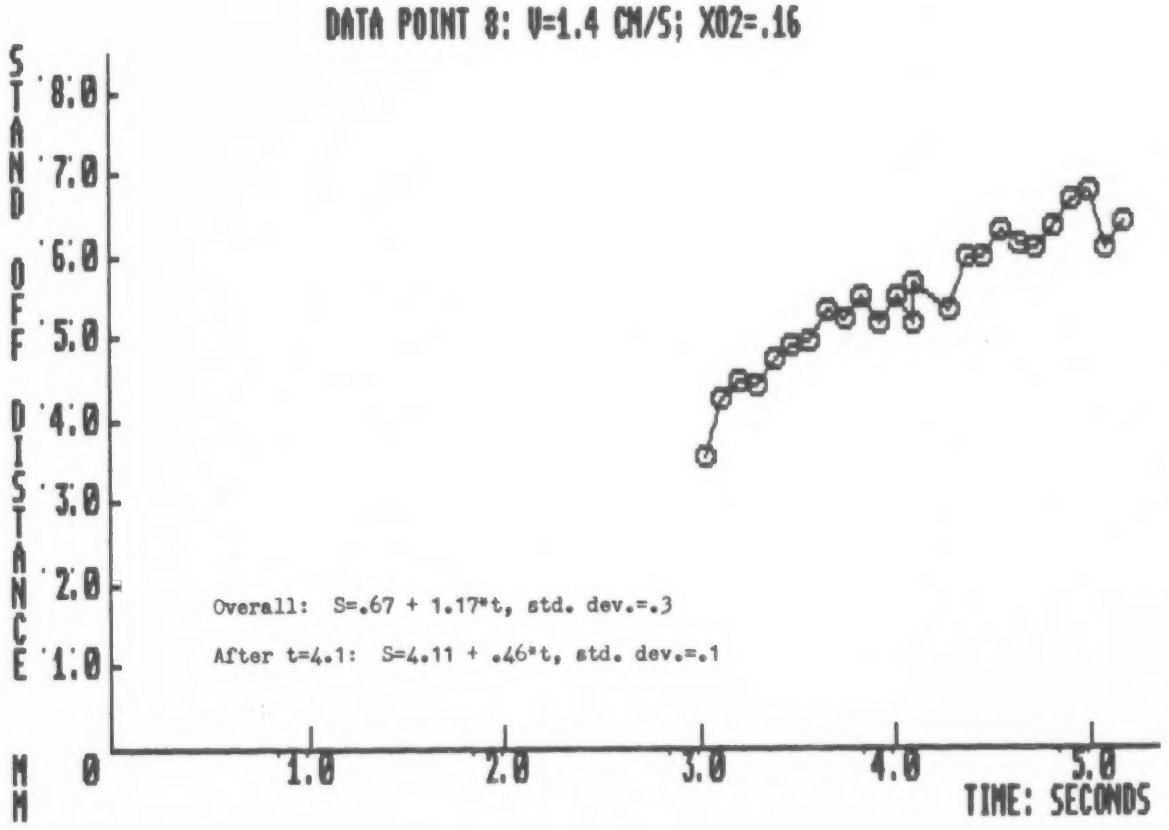

Figure C.4. Stand off distance versus time for data point 8.

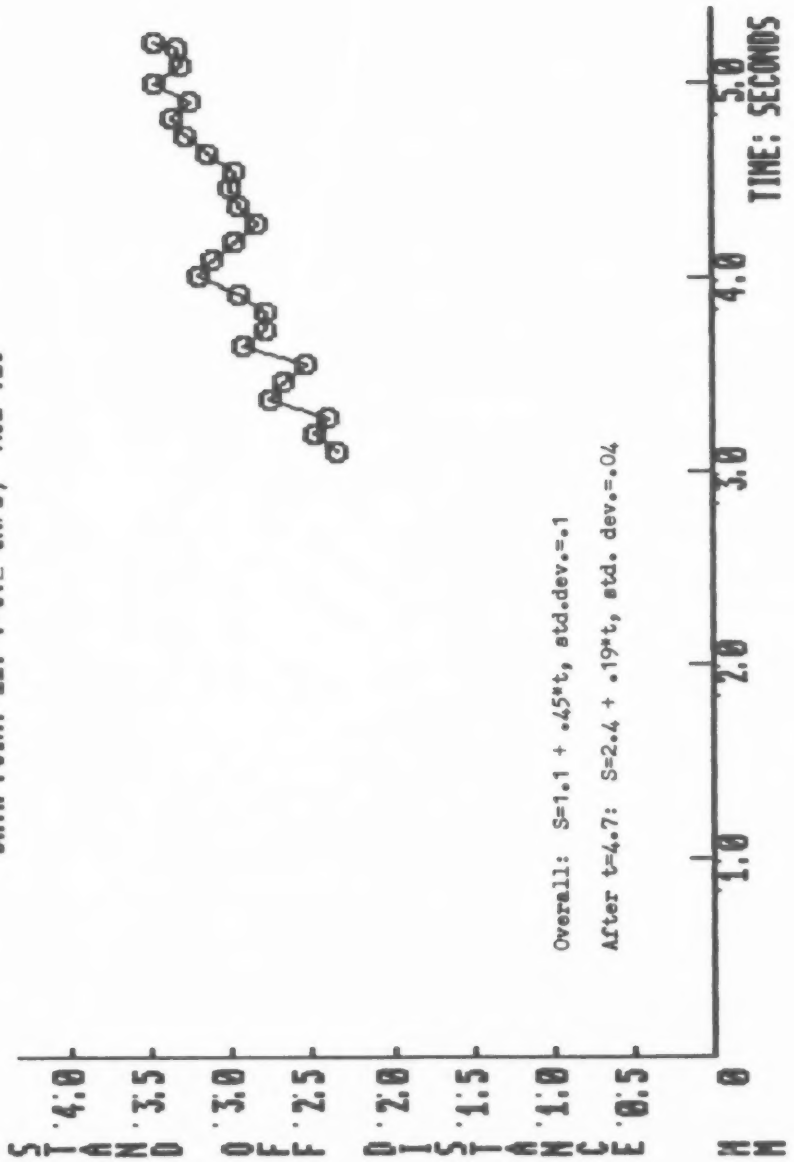

Figure C.5. Stand off distance versus time for data point 11.

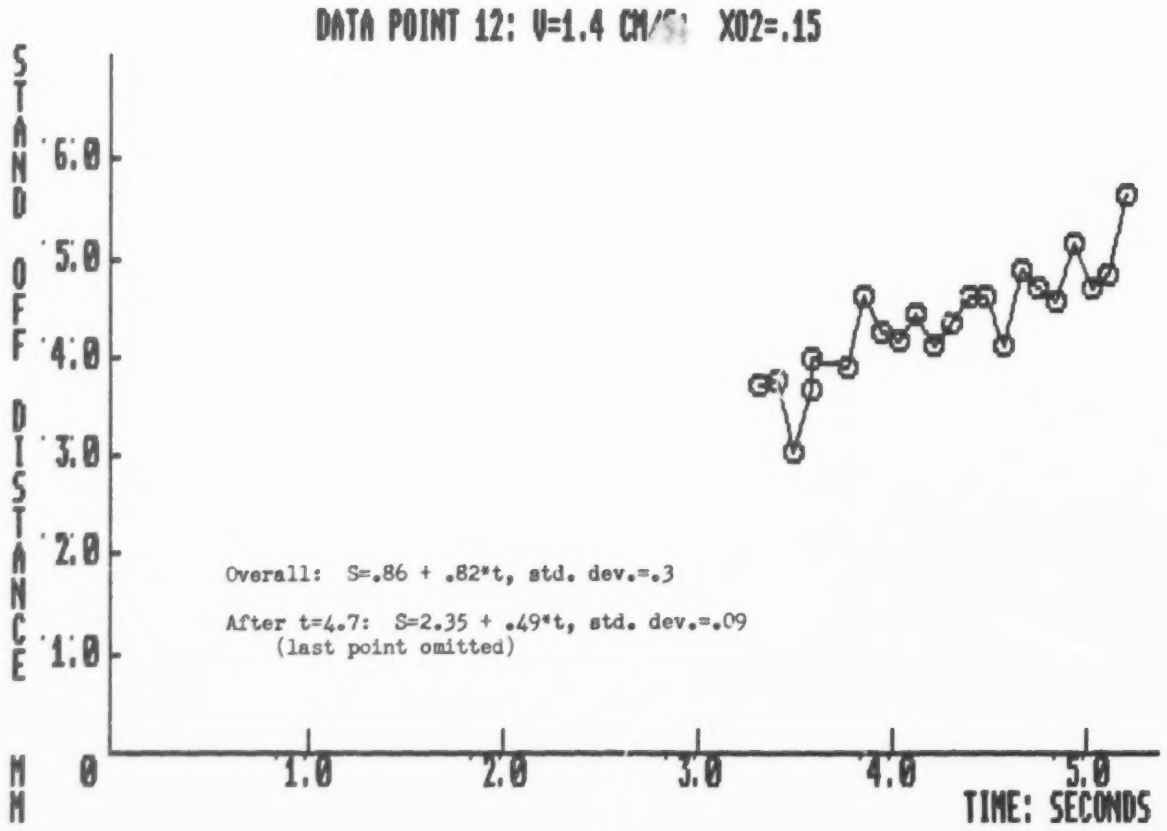

Figure C.6. Stand off distance versus time for data point 12.

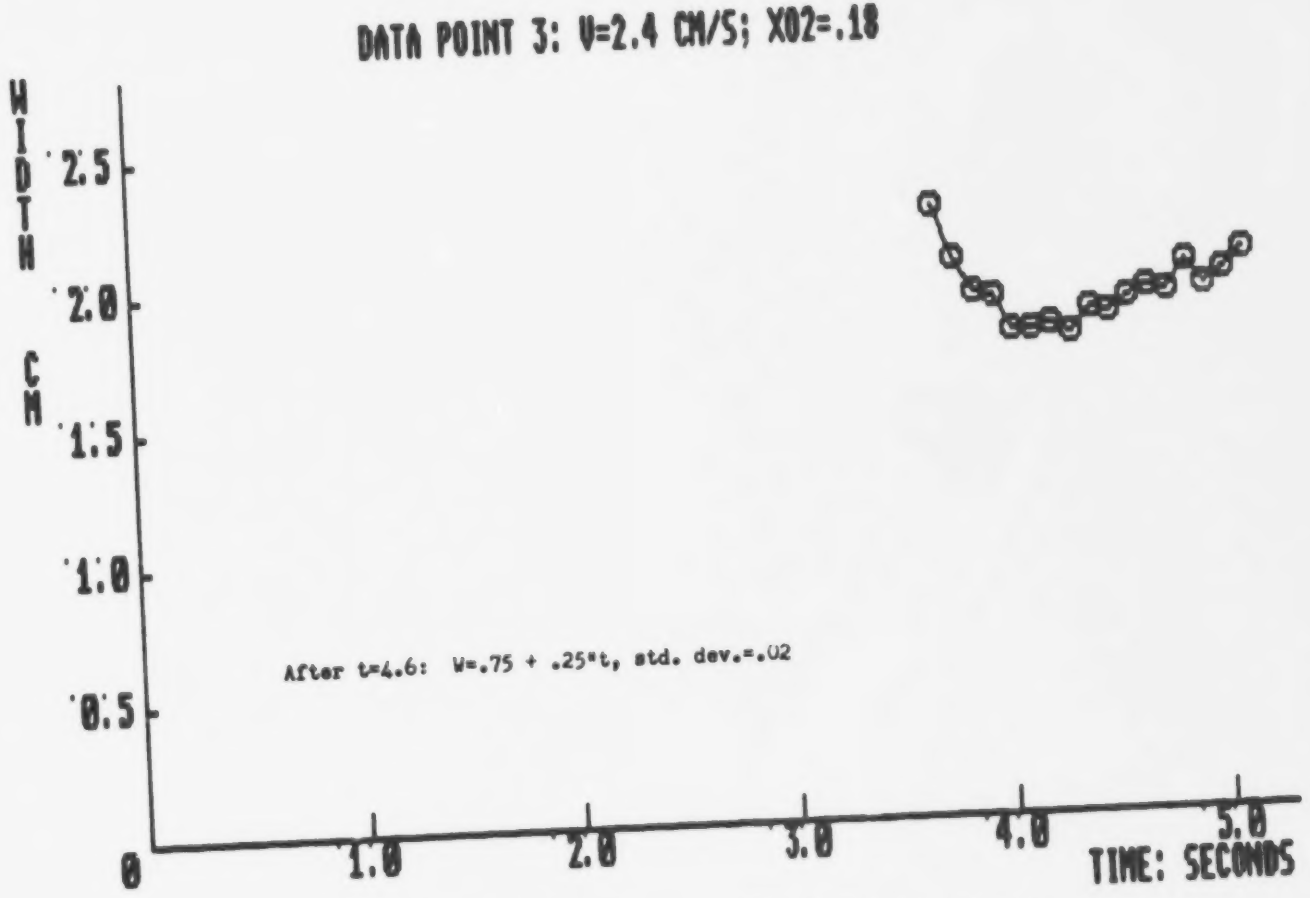

Figure C.7. Flame width versus time for data point 3.

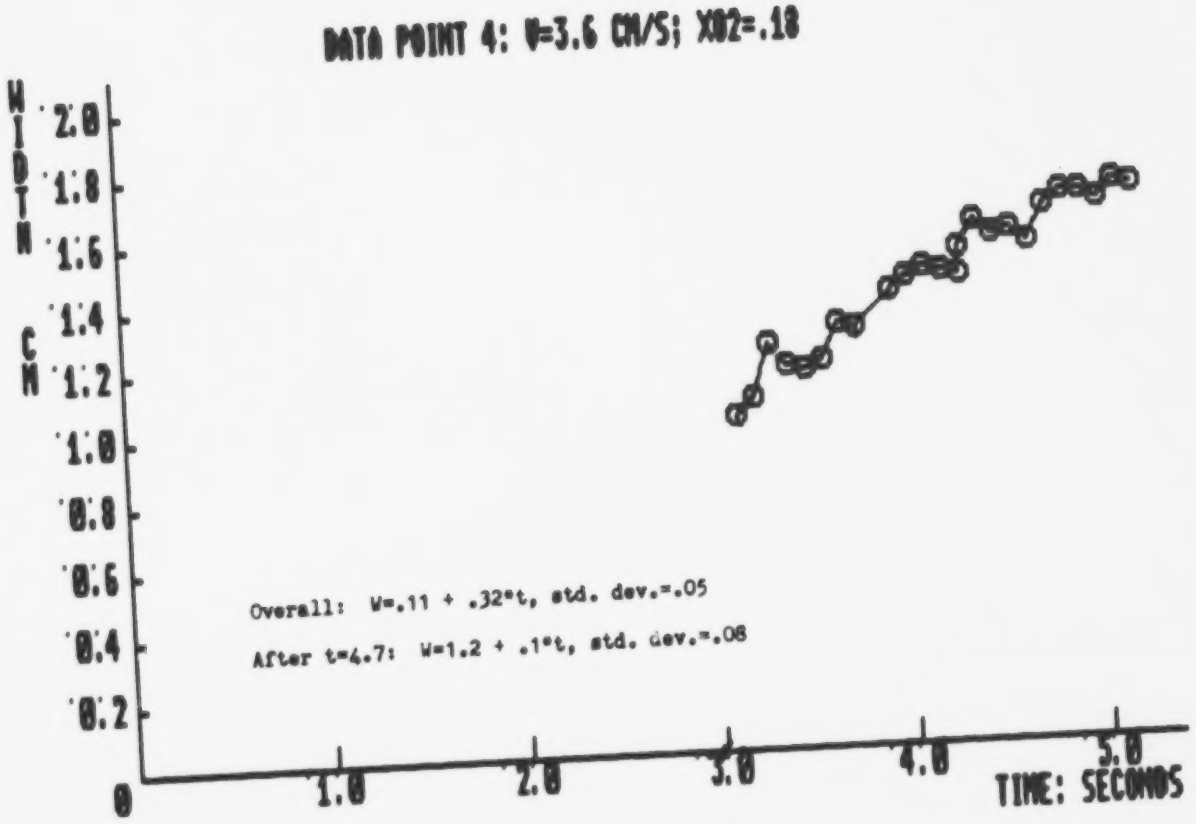

Figure C.8. Flame width versus time for data point 4.

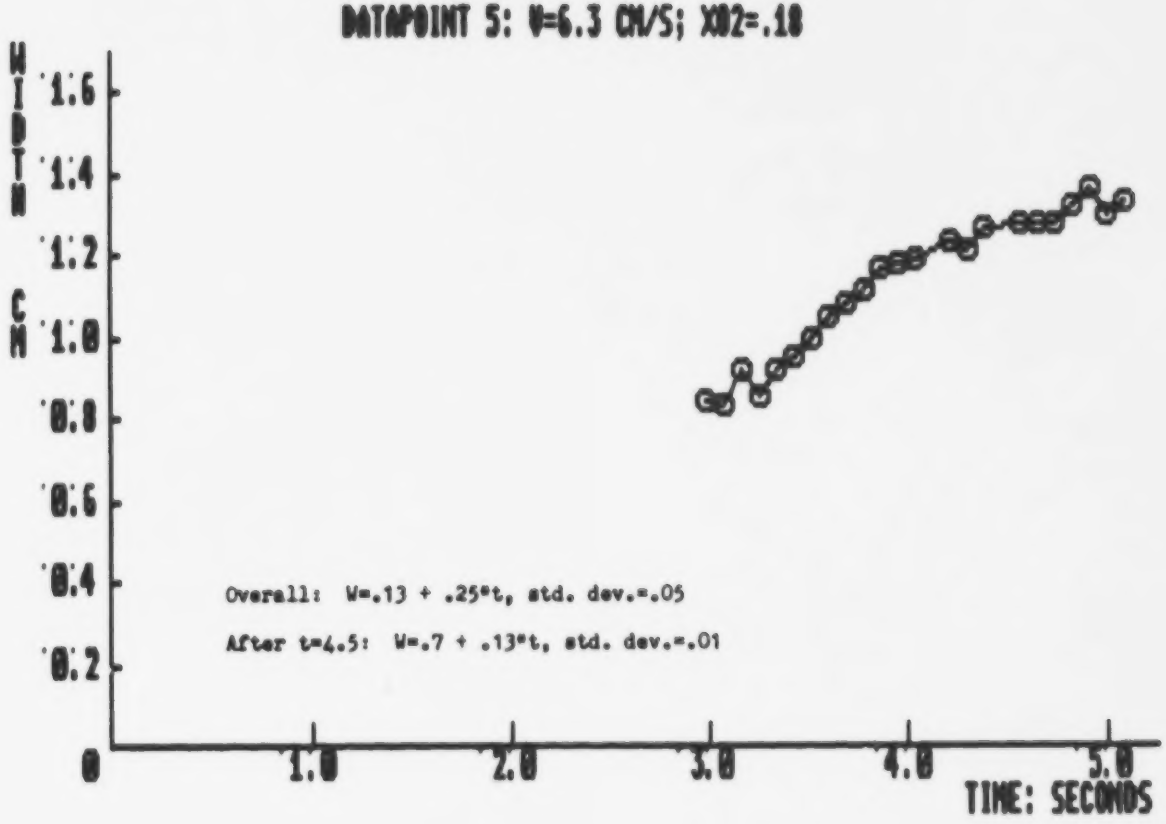

Figure C.9. Flame width versus time for data point 5.

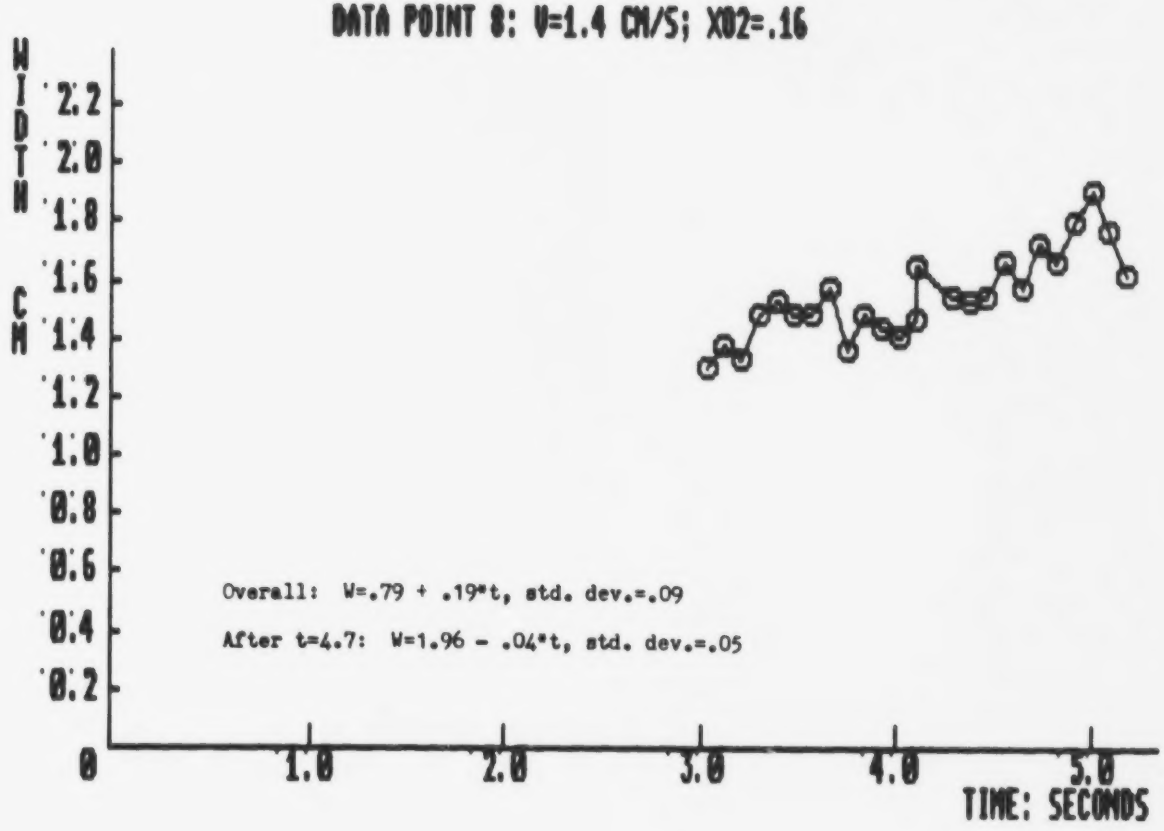

Figure C.10. Flame width versus time for data point 8.

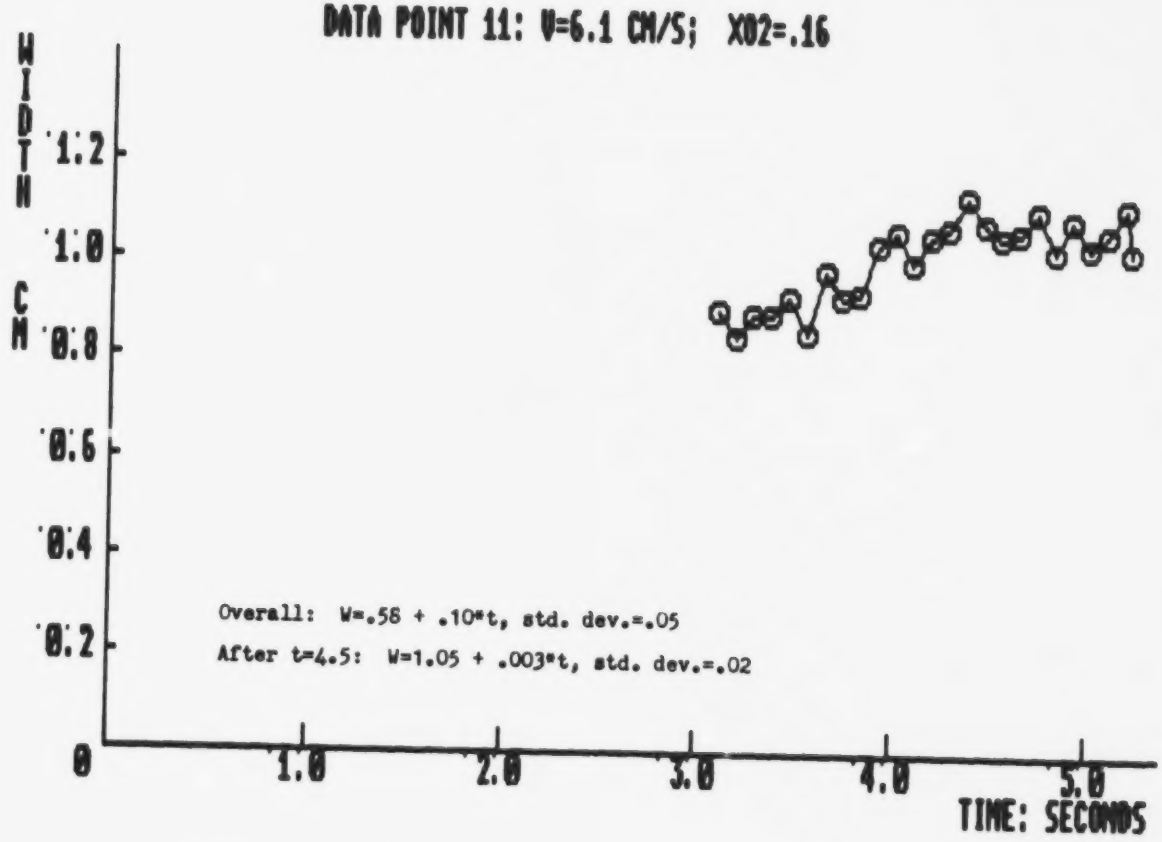

Figure C.11. Flame width versus time for data point 11.

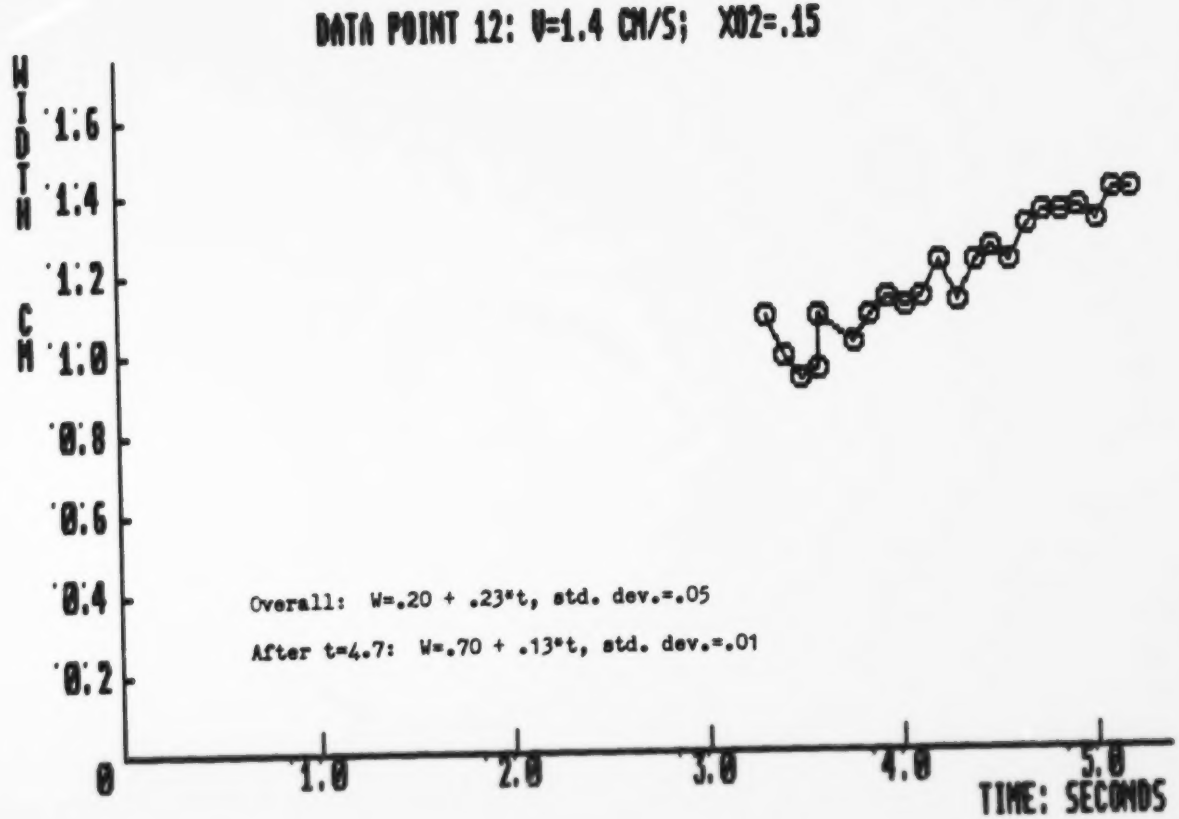

Figure C.12. Flame width versus time for data point 12.

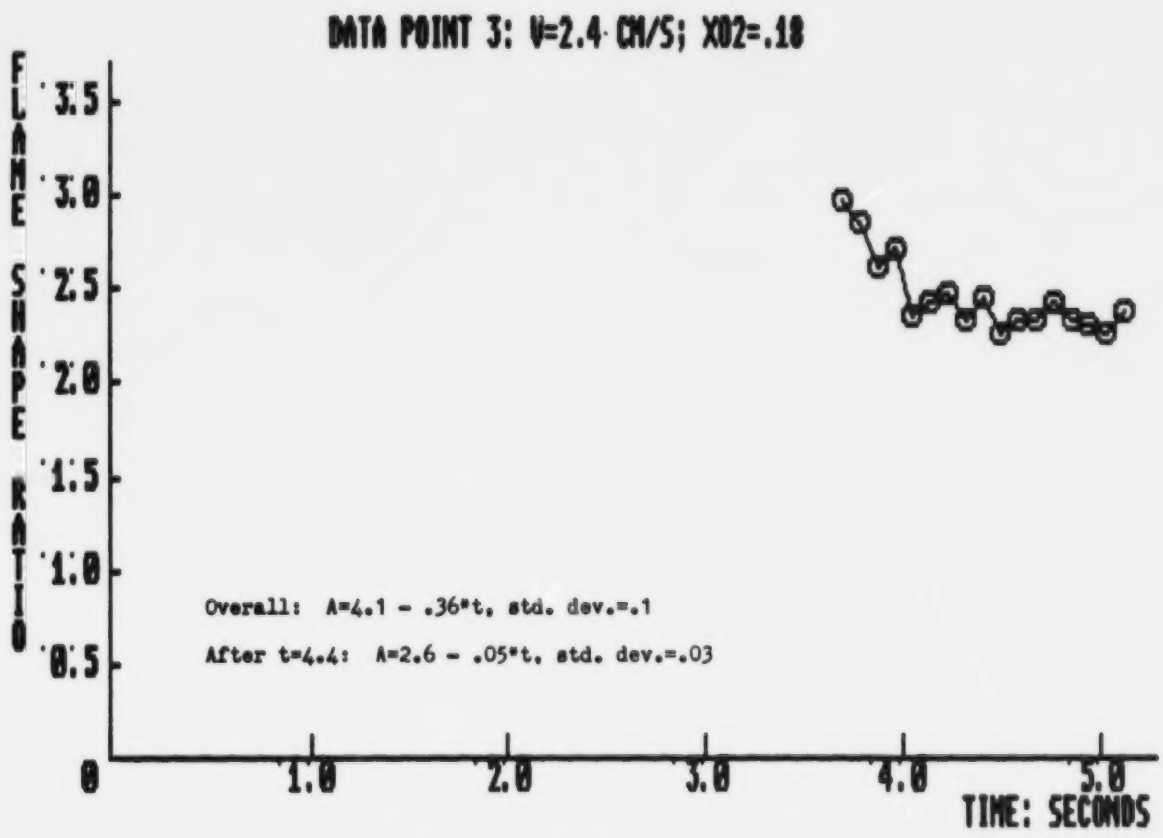

Figure C.13. Flame shape ratio versus time for data point 3.

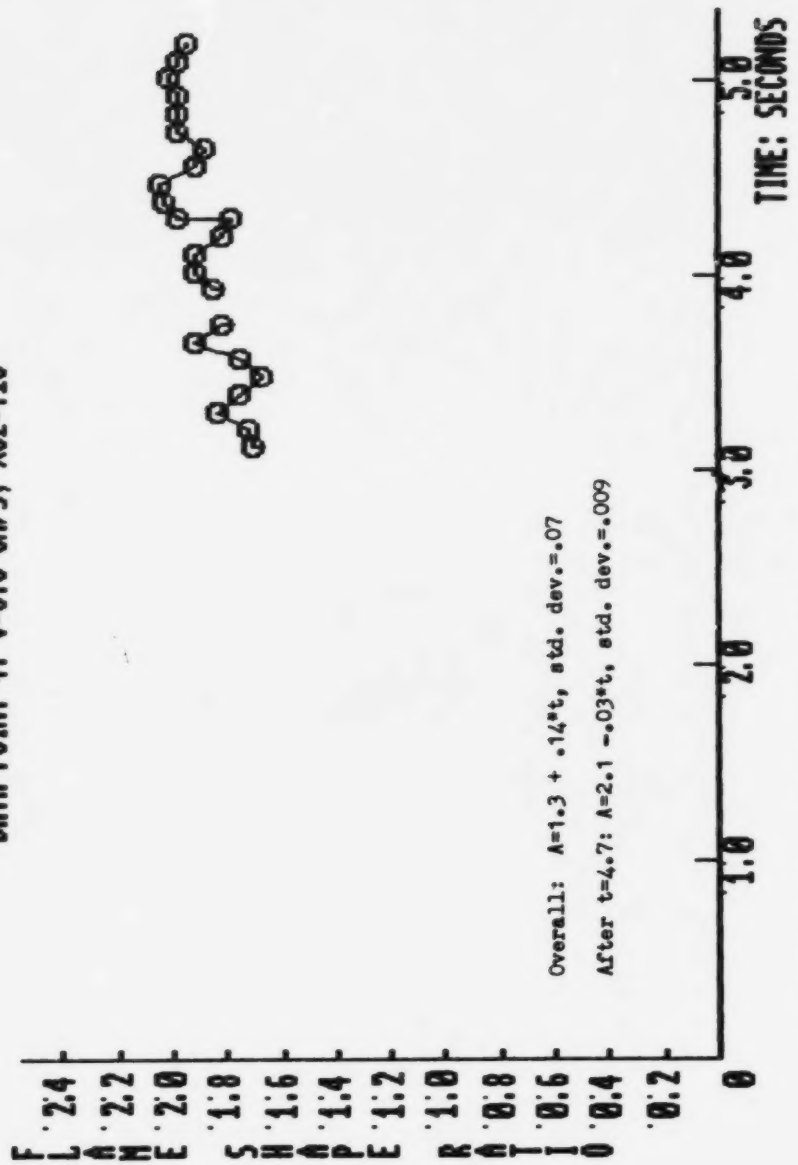

Figure C.14. Flame shape ratio versus time for data point 4.

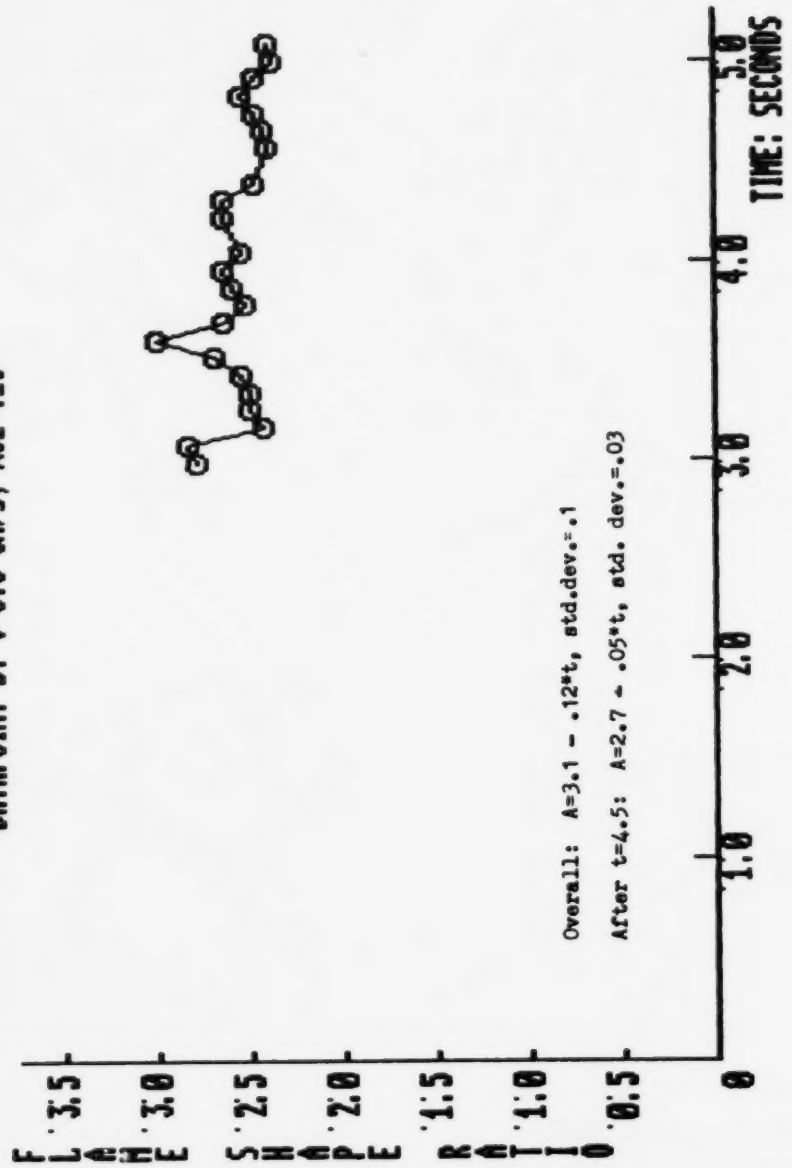

Figure C.15. Flame shape ratio versus time for data point 5.

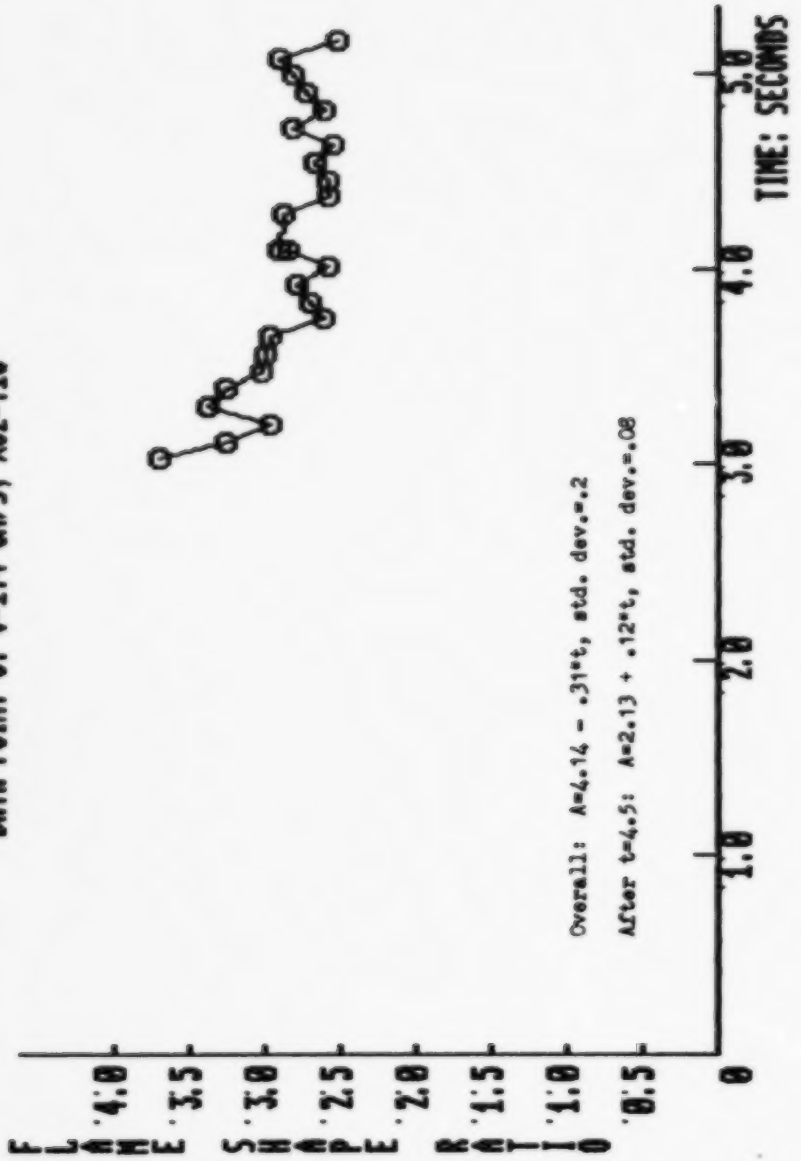

Figure C.16. Flame shape ratio versus time for data point 8.

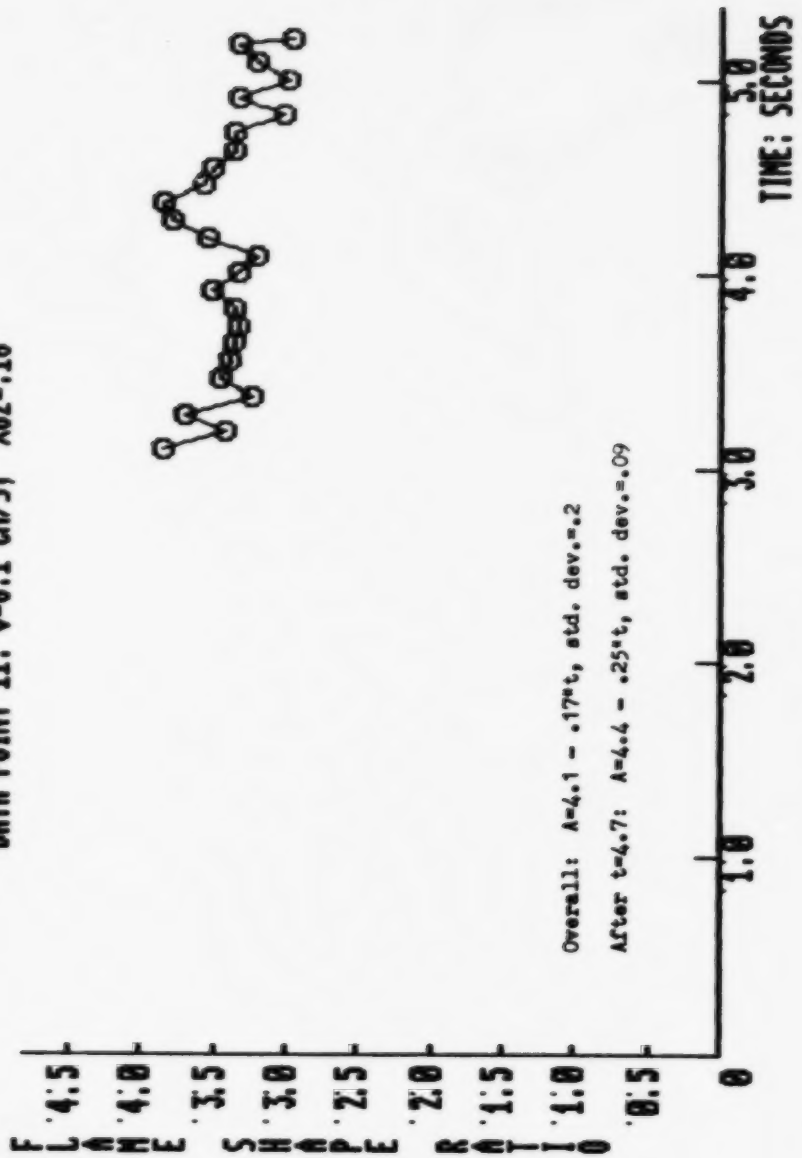

Figure C.17. Flame shape ratio versus time for data point 11.

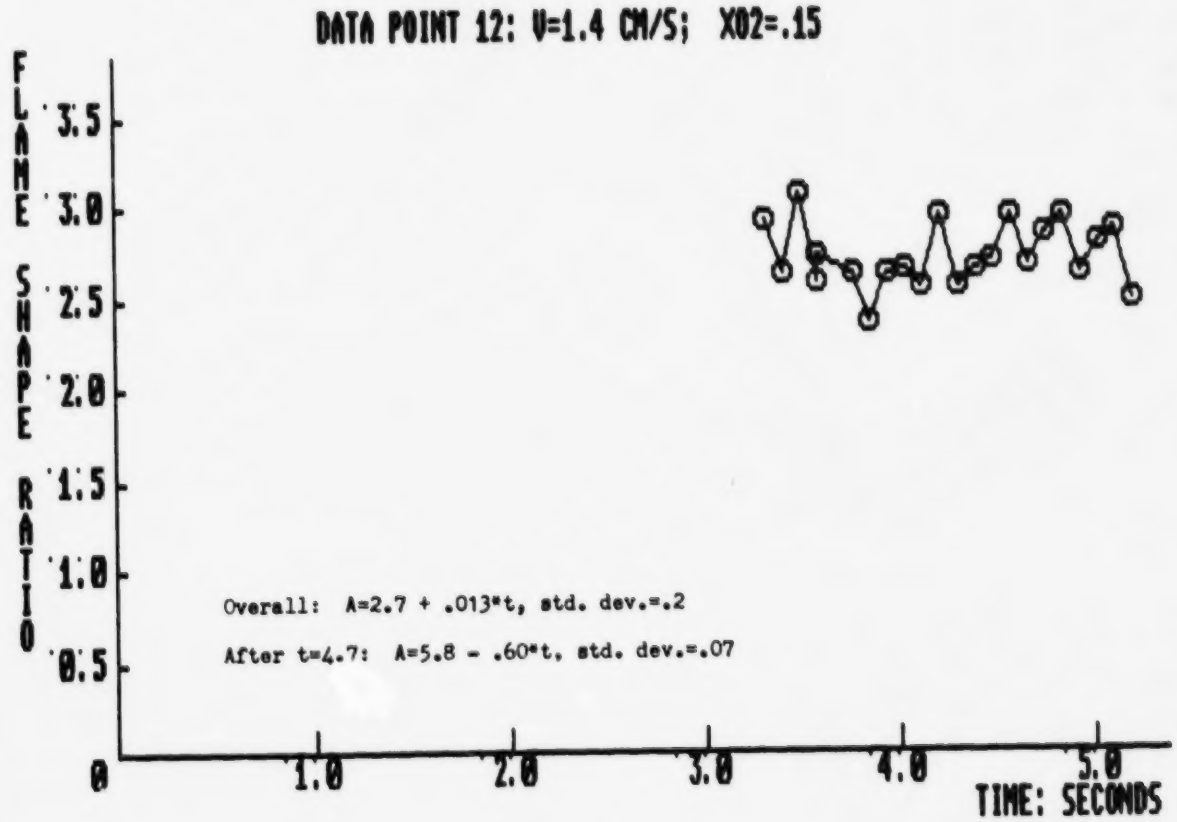

Figure C.18. Flame shape ratio versus time for data point 12.

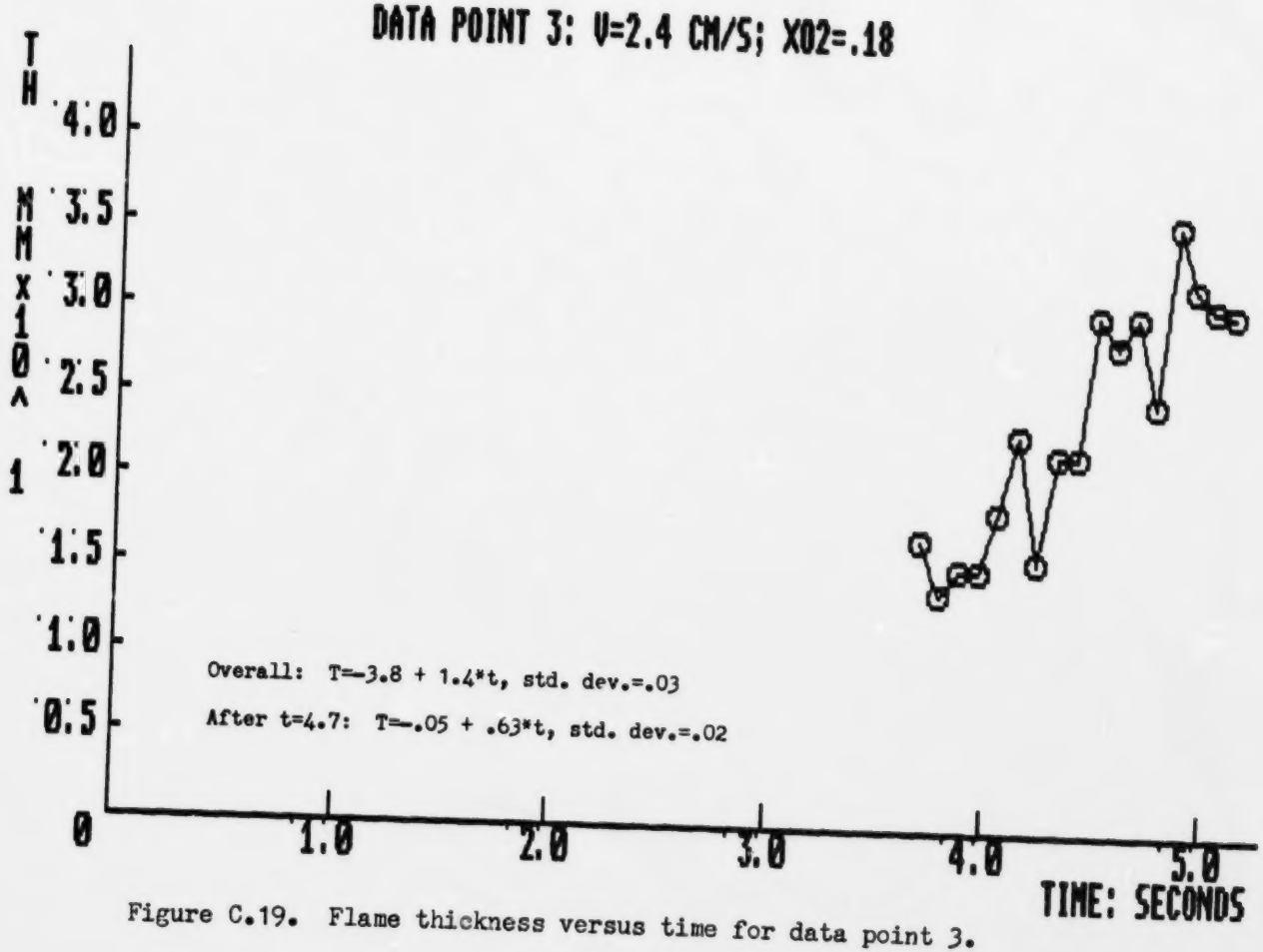

Figure C.19. Flame thickness versus time for data point 3.

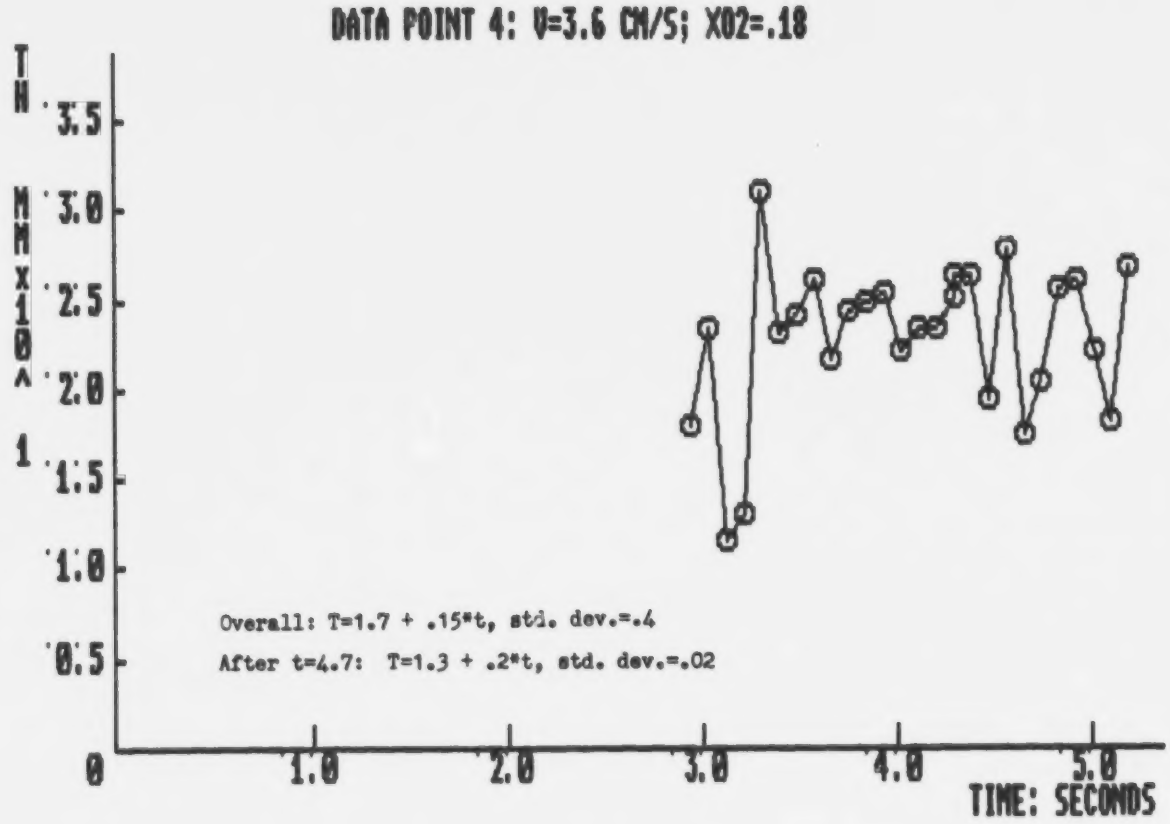

Figure C.20. Flame thickness versus time for data point 4.

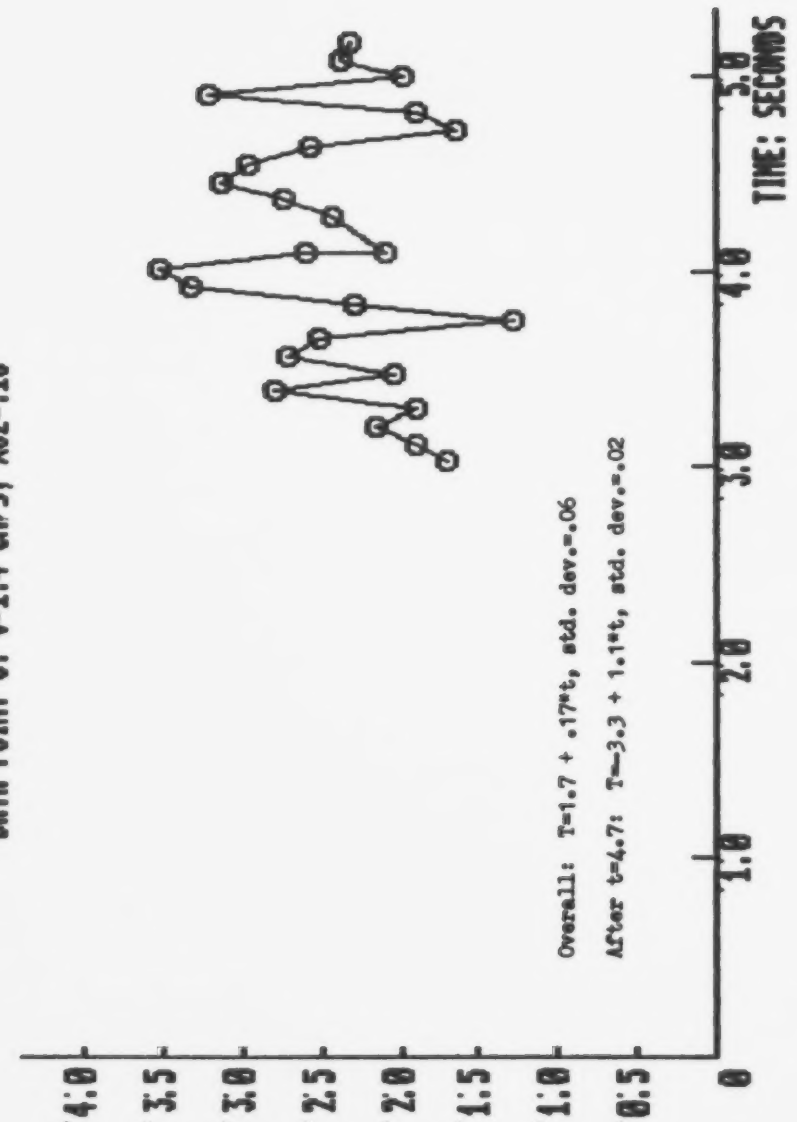

Figure C.21. Flame thickness versus time for data point 8.

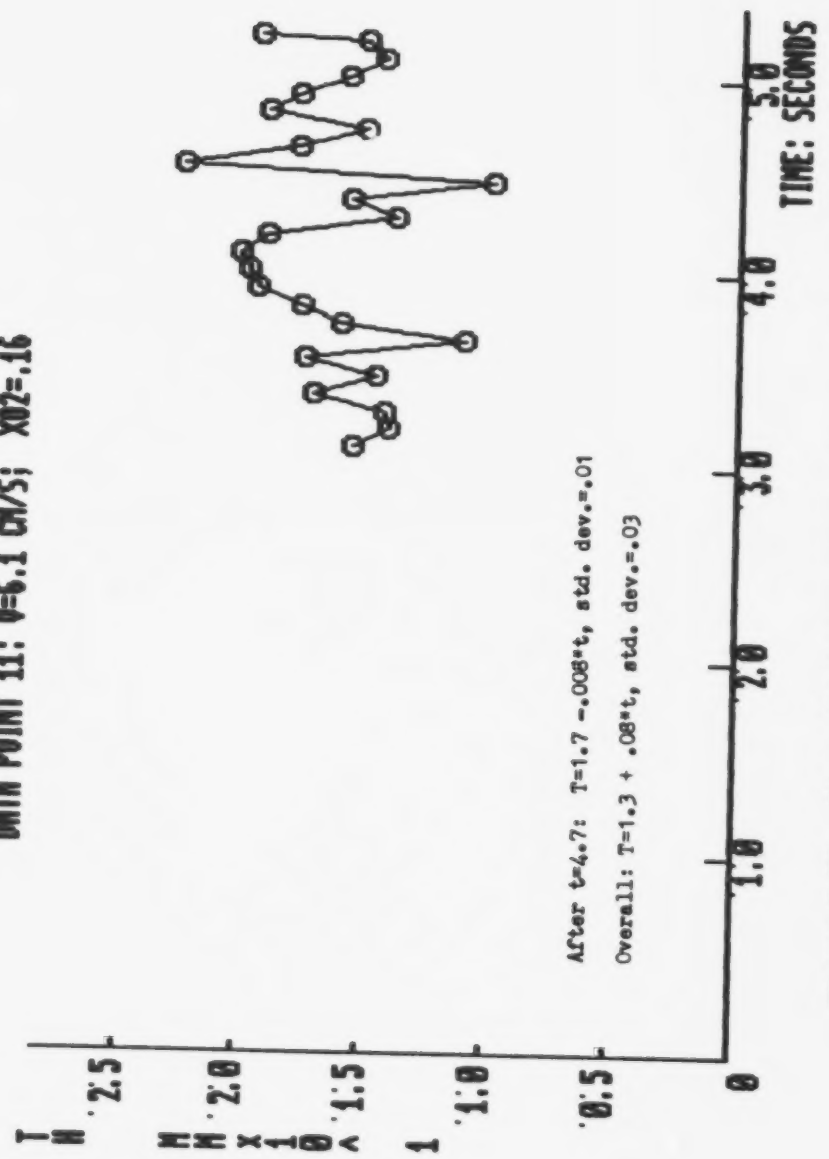

Figure C.22. Flame thickness versus time for data point 11.

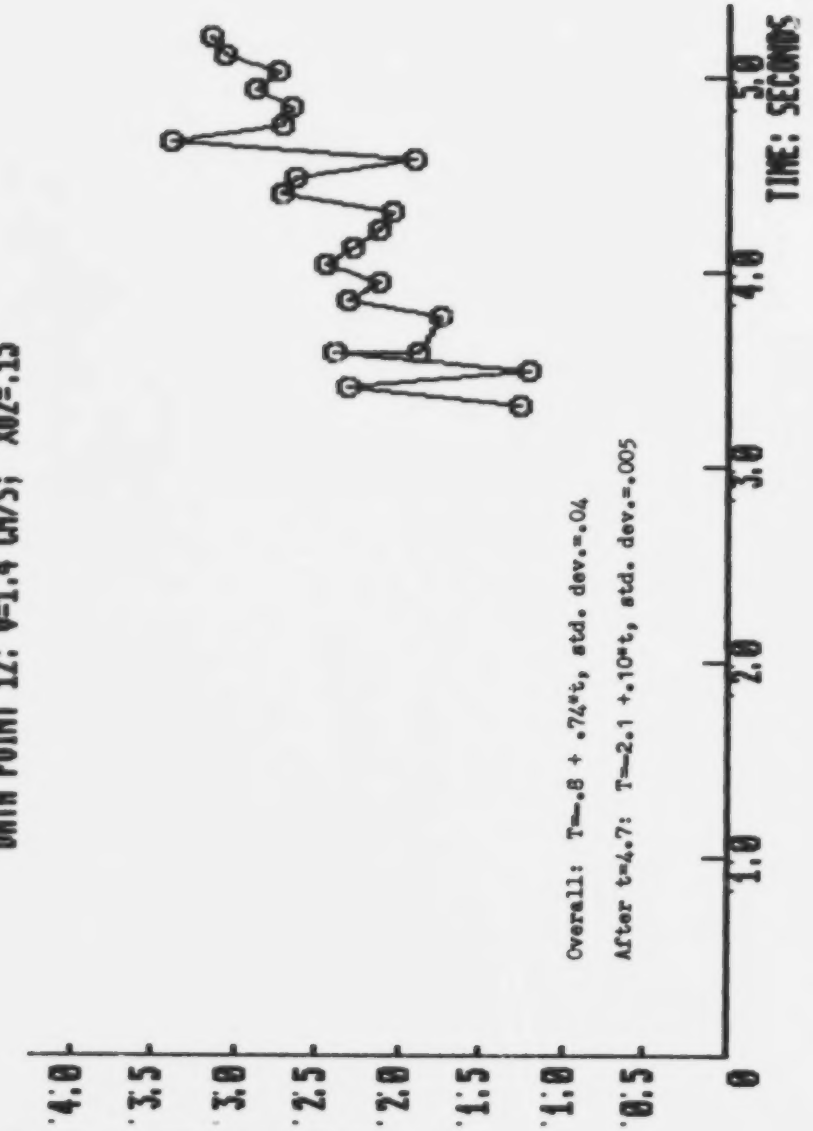

Figure C.23. Flame thickness versus time for data point 12.

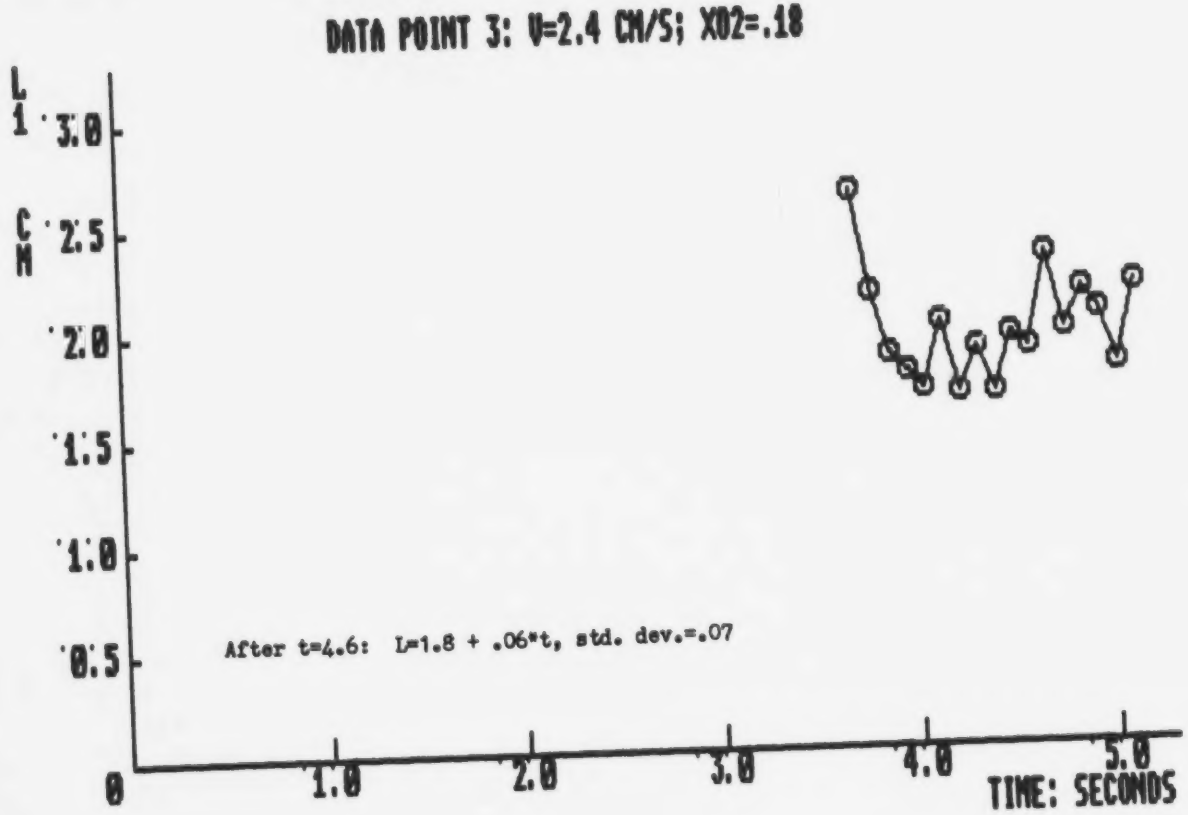

Figure C.24. Flame length versus time for data point 3.

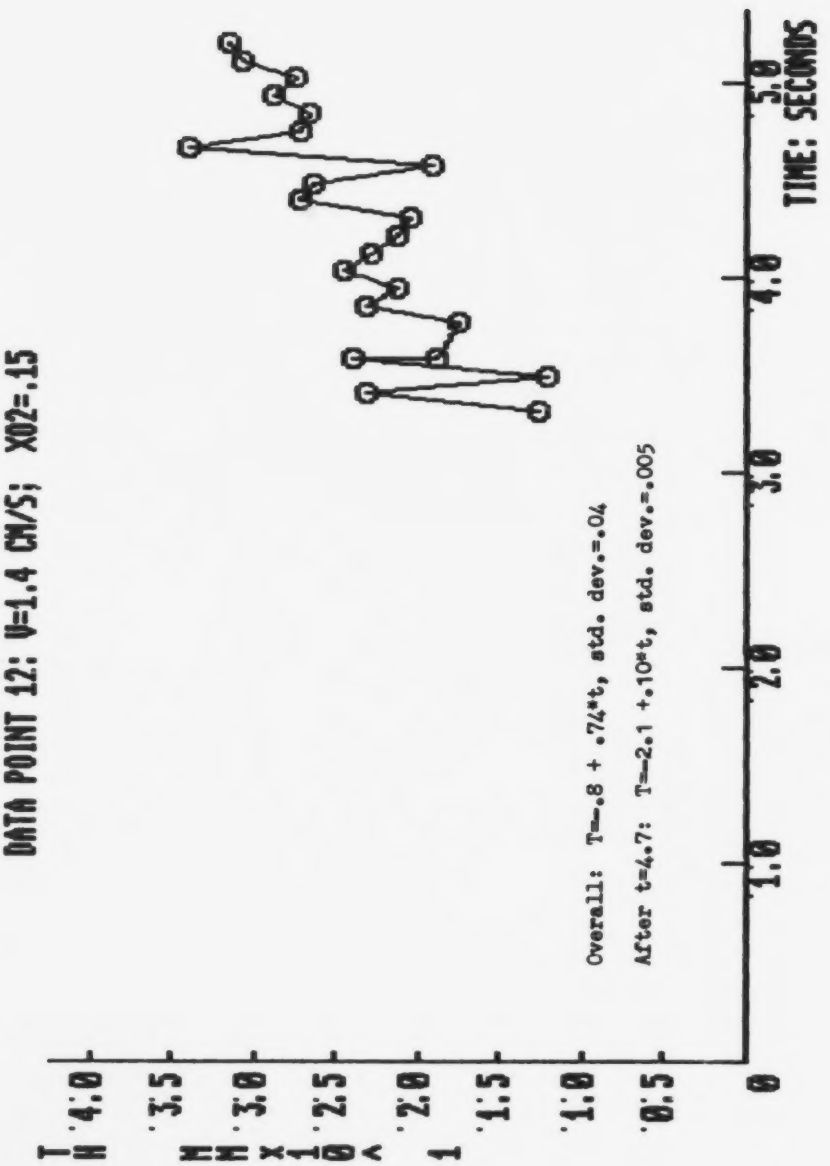

Figure C.23. Flame thickness versus time for data point 12.

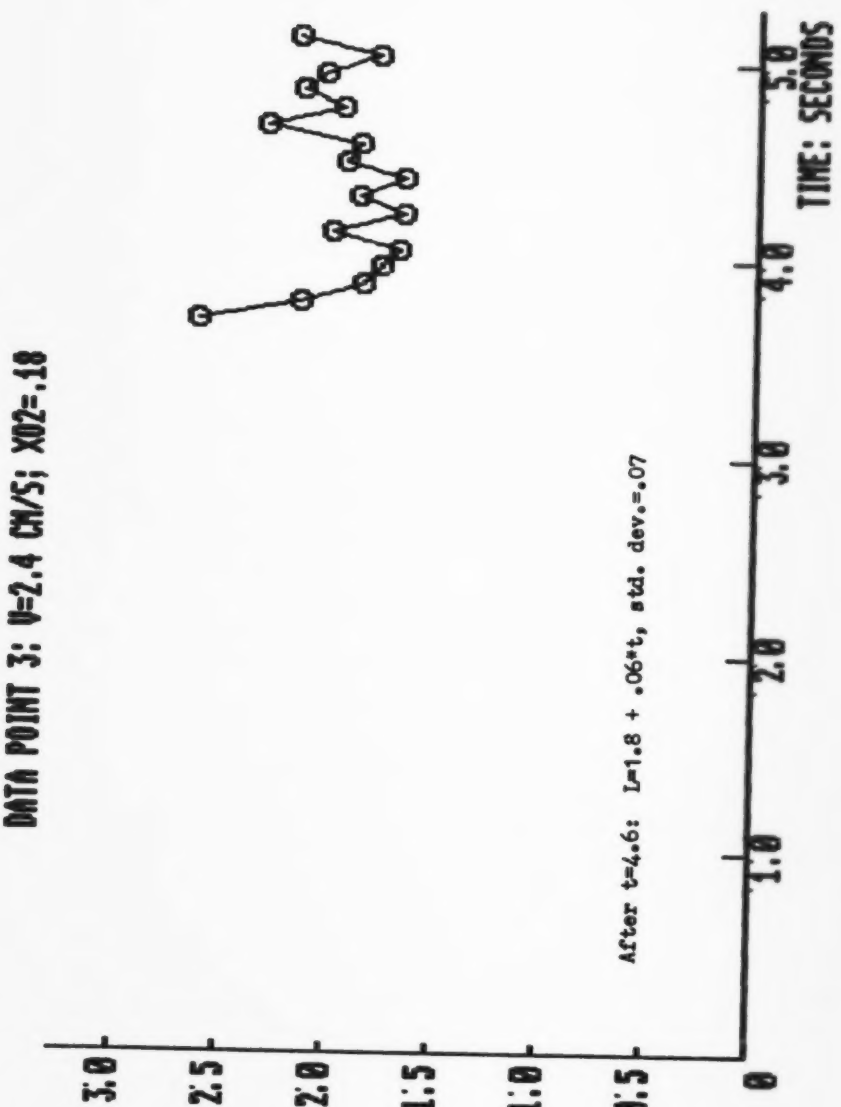

Figure C.24. Flame length versus time for data point 3.

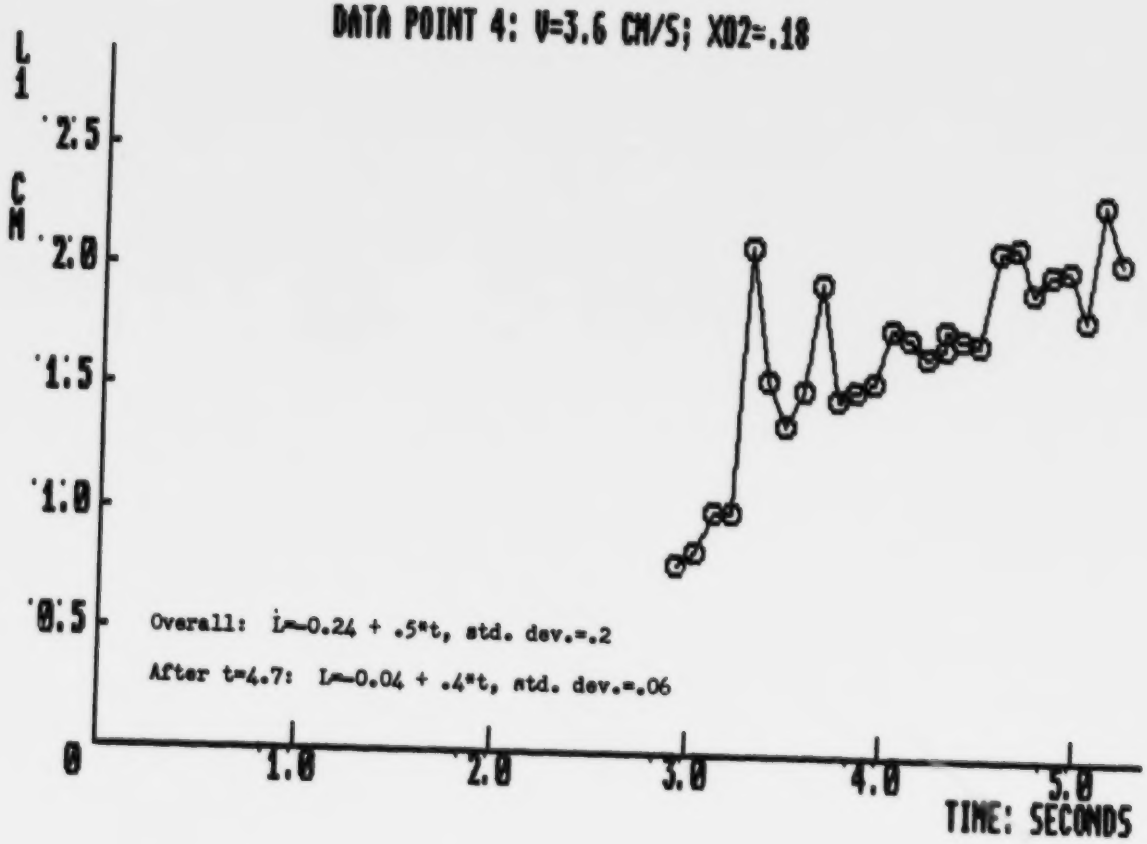

Figure C.25. Flame length versus time for data point 4.

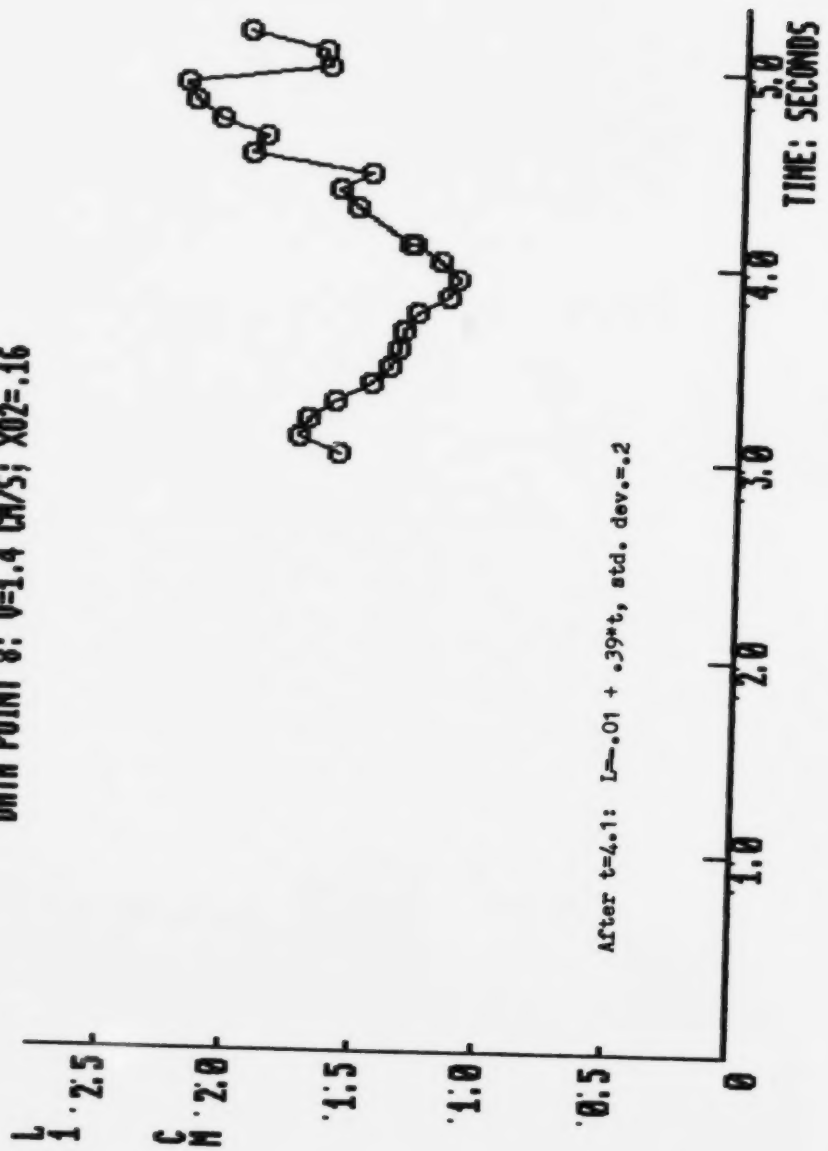

Figure C.26. Flame length versus time for data point 8.

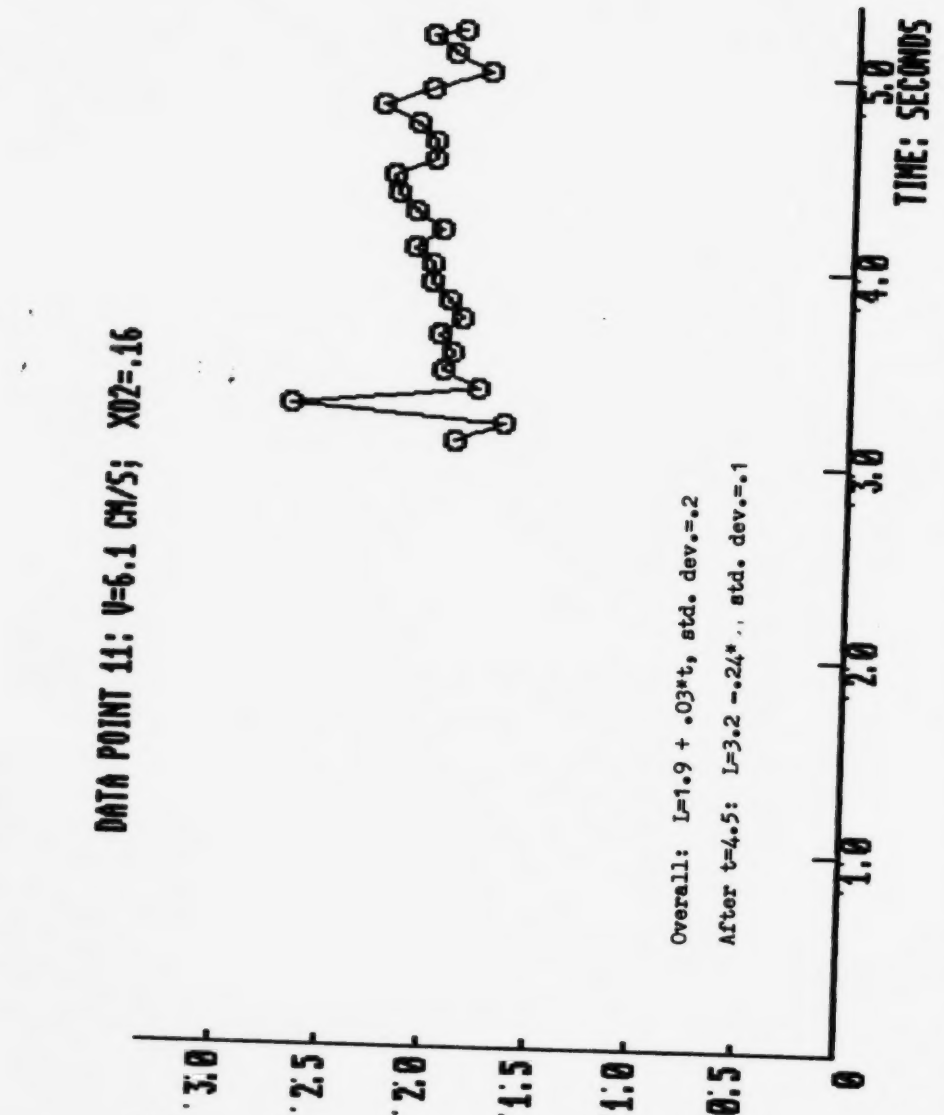

Figure C.27. Flame length versus time for data point 11.

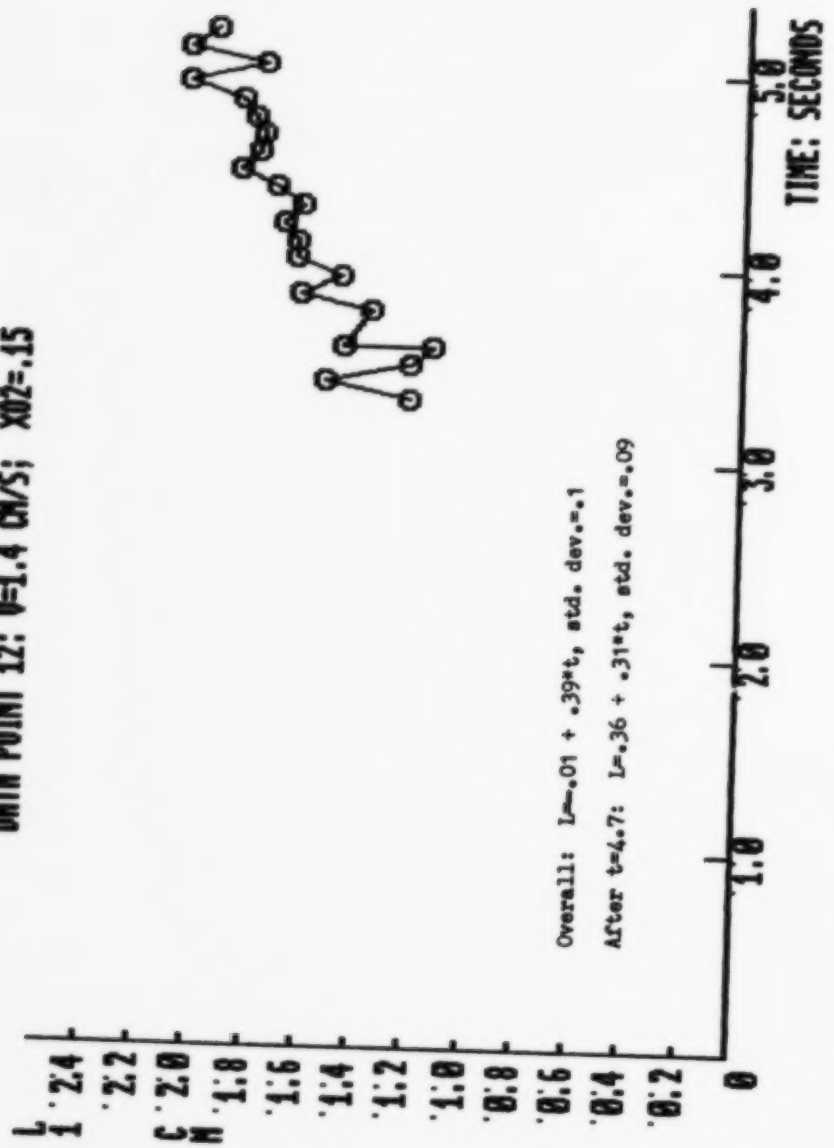

Figure C.28. Flame length versus time for data point 12.

1. Report No.	2. Government Accession No.	3. Recipient's Catalog No.
NASA CR-179576		

4. Title and Subtitle	5. Report Date
Size and Shape of Solid Fuel Diffusion Flames in Very Low Speed Flows	April 1987
	6. Performing Organization Code

7. Author(s)	8. Performing Organization Report No.
David W. Foutch	None
	10. Work Unit No. 674-22-05

9. Performing Organization Name and Address	11. Contract or Grant No.
Case Western Reserve University Dept. of Mechanical and Aerospace Engineering Cleveland, Ohio 44106	NGT-36-027805
	13. Type of Report and Period Covered Contractor Report Final

12. Sponsoring Agency Name and Address	14. Sponsoring Agency Code
National Aeronautics and Space Administration Lewis Research Center Cleveland, Ohio 44135	

15. Supplementary Notes

Project Manager, Sandra L. Olson, Space Experiments Division, NASA Lewis Research Center. This report was submitted as a thesis in partial fulfillment of the requirements for the Degree of Master of Science to Case Western Reserve University in January 1987.

16. Abstract

The effect of very low speed forced flows on the size and shape of a solid fuel diffusion flame are investigated experimentally. Flows due to natural convection are eliminated by performing the experiment in low gravity. The range of velocities tested is 1.5 cm/s to 6.3 cm/s and the mole fraction of oxygen in the O_2/N_2 atmosphere ranges from 0.15 to 0.19. The flames did not reach steady state in the 5.2 sec to which the experiment was limited. Despite limited data, trends in the transient flame temperature and, by means of extrapolation, the steady state flame size are deduced. As the flow velocity is reduced, the flames move farther from the fuel surface, and the transient flame temperature is lowered. As the oxygen concentration is lowered the flames move closer to the fuel sample and the transient flame temperature is lowered. With stand off distances up to 8.5 ± 0.7 mm and thicknesses around 1 or 2 mm, these flames are much weaker than flames observed at normal gravity. Based on the performance of the equipment and several qualitative observations, suggestions for future work are made.

17. Key Words (Suggested by Author(s))	18. Distribution Statement
Flammability Zero gravity Spacecraft fire safety Combustion	Unclassified - unlimited STAR Category 28

19. Security Classif. (of this report)	20. Security Classif. (of this page)	21. No. of pages	22. Price*
Unclassified	Unclassified	117	A06

*For sale by the National Technical Information Service, Springfield, Virginia 22161